Unprecedented Partial Paddlewheel Dirhodium Methyl Isocyanide Compounds with Unusual Structural and Electronic Properties: A Comprehensive Experimental and Theoretical Study

Zhanyong Li, Helen T. Chifotides, Kim R. Dunbar*

Supplementary Information

Experimental Section, Syntheses of Starting materials and Compounds **2**, **3**, **5**-**8**, NMR studies, X-ray Crystallographic and Computational Information, TD-DFT Calculations for **3** and **7**, References

List of Figures

Fig. S1 ^{1}H-NMR spectra for **2** in CD_3CN at different time intervals.

Fig. S2 ^{1}H-NMR spectrum of **5** in CD_3CN recorded 10 min after dissolving it.

Fig. S3 Aliphatic region of the ^{1}H-NMR spectra for **8** in CD_3CN at different time intervals.

Fig. S4 ^{31}P {^{1}H}-NMR spectra of **8** in CD_3CN obtained at different time intervals.

Fig. S5 Thermal ellipsoid plot for the cationic unit in **2** at 50% probability level.

Fig. S6 Thermal ellipsoid plot for the cationic unit in **3** at 50% probability level.

Fig. S7 Thermal ellipsoid plot of **8**-*R* at the 50% probability level.

Fig. S8 Gas phase optimized structures for **1**-**8**.

Fig. S9 Diagrams of the MO levels for the dirhodium units in **2** and **6**.

Fig. S10 Representation of the orbital interactions between $Rh_2(\delta^*)$, $p\pi$ lone pairs on the bridging ligand and the low lying π^*orbital on the CH_3NC ligands.

Fig. S11 Diagram of the MO levels for the dirhodium unit in **8**.

Fig. S12 and **Fig. S13** Overlay of experimental and calculated electronic absorption spectra for **1**-**4, 5**-**8**.

Fig. S14 and Fig. S15 Visualization of the frontier molecular orbitals in **1**-**4** and **5**-**8**.

Scheme S1. Representation of the **R** and **S** isomers in compound **8**.

List of Tables

Table S1. Important bond distances and dihedral angles for the optimized and crystallographically determined structures of **1**-**8**.

Tables S2, S3 and S5. Bond Character of Orbitals, Energy Levels and orbital composition (%) for the dirhodium units in **1**/**5**, **3**/**7** and **8**, respectively.

Table S4. Orbital composition (%) for compounds **1**-**8**.

Tables S6-S9. Excited states calculated by TD-DFT/PCM for **1**/ **2**, **5**/ **6**, **3**/ **7** and **4**/ **8**, respectively.

Table S10. The ν(CN) (cm^{-1}) for the CH_3CN stretches in the free ligand and **1**-**4**.

Experimental Section

Physical Measurements. The ^{1}H NMR spectroscopic data were collected on a 300 MHz Varian spectrometer. The ^{1}H NMR spectra were referenced relative to the residual proton impurities of the deuterated solvent (CD_3CN-d_3) and the ^{31}P-{^{1}H} NMR spectra were referenced to H_3PO_4 in D_2O (30% w/w), which was used as an external reference (0 ppm). Infrared spectra were recorded as Nujol mulls between KBr plates with a Nicolet Nexus 470 FT-IR spectrometer. Electronic absorption (UV-vis) spectra were acquired with a Shimadzu UV-1601PC spectrophotometer. Electrochemical data were collected using a CH Instruments analyzer. The cyclic voltammetry data were obtained in dry CH_3CN with 0.10 M [n-Bu_4N][PF_6] as the supporting electrolyte at 25 ºC. The $E_{1/2}$ values [$E_{1/2} = (E_{p,a} + E_{p,c})/2$] were referenced to the Ag/AgCl electrode without correction for the junction potentials. The $FeCp_2$/[$FeCp_2$]$^{+}$ couple occurs at $E_{1/2}$ = + 0.48 V in CH_3CN at the same conditions used for the compounds. Elemental analyses were performed by Atlantic Microlab, Inc. Electrospray mass spectrometry data were obtained by the Laboratory for Biological Mass Spectrometry at Texas A&M University using a PE Sciex (Concord, Ontario, Canada) API Qstar Pulsar with an Ionworks time-to-digital converter TDC x 4 for data recording.

Starting Materials. The precursor [RhCl(COD)]$_2$ (COD: cycloocta-1,5-diene) was purchased from Pressure Chemicals whereas [$FeCp_2$][BF_4] and [RhCl(CO)$_2$]$_2$ were purchased from Sigma-Aldrich; all reagents were used as received. Methyl isocyanide (CH_3NC),[1] and NNNH (ditolyl-triazene)[2] and the rhodium complexes [Rh(F-form)(COD)]$_2$,[3] [Rh(NNN)(CO)$_2$]$_2$ were prepared according to published procedures.[4] Acetonitrile was pre-dried over 3 Å molecular sieves and distilled under N_2. Dichloromethane was pre-dried over 4 Å molecular sieves and distilled over P_2O_5 under N_2. All manipulations were conducted using standard Schlenk-line techniques unless otherwise stated. The work-up and isolation of the products was conducted in air.

Syntheses. Preparation of *cis*-[Rh$_2$(F-form)$_2$(CH$_3$CN)$_6$][BF$_4$]$_2$ (2). A quantity of [Rh(F-form)(COD)]$_2$ (120 mg, 0.136 mmol) was added to 30 mL of CH_2Cl_2:CH_3CN (1:1 v/v) and the red/orange solution was stirred until the solid was fully dissolved. Subsequently $AgBF_4$ (106 mg,

0.547 mmol) was added to the solution and the color was noted to gradually change to green. The reaction solution was stirred in the dark at room temperature for 24 h and then filtered through Celite® to remove finely divided silver particles. The filtrate was evaporated to dryness and redissolved in 10 mL of CH_3CN (red solution). The addition of diethyl ether (40 mL) induced precipitation of the desired product. Yield: 112 mg, 75%. Found: C, 36.67; N, 10.33; H, 3.11%. Calc. for $C_{38}H_{36}N_{10}B_2F_{12}Rh_2 \bullet 3CH_2Cl_2$: C, 36.64; N, 10.43; H, 3.15 %. δ_H (300 MHz; CD_3CN-d_3) 2.53 (12 H, s, eq CH_3CN), 7.05 (16 H, m, *p*-difluorophenyl), 7.49 (2 H, t, NCHN, $^3J_{Rh\text{-}H}$ = 4 Hz). UV-vis, $\lambda_{max}(CH_3CN)$/nm 254 (ε x 10^3 /dm^3 mol^{-1} cm^{-1} 47.5), ~312 (7.4), ~416 (0.85), ~510 (0.4). IR (Nujol mull) ν_{CN}/cm^{-1}: 2334(w), 2308(m), 2276(w). Cyclic Voltammetry (CV/V, vs Ag/AgCl in ~ 0.10 M [*n*-Bu_4N][PF_6]): $E_{1/2}(red)_1$ -0.47, $E_{1/2}(red)_2$ -1.26, $E_{1/2}(ox)_1$ +1.13, $E_{1/2}(ox)_2$ +1.63.

Preparation of *cis*-[$Rh_2(NNN)_2(CH_3CN)_6$][BF_4]$_2$ (3). Samples of [$RhCl(CO)_2$]$_2$ (50 mg, 0.13 mmol) and 58 mg (0.26 mmol) of NNNH were added to dry CH_2Cl_2 (25 mL). After dissolution of the two reactants, NEt_3 (45 μL, 0.32 mmol) was added to the solution which was accompanied by an instantaneous color change from yellow to red. The reaction solution was stirred under N_2 for 20 minutes and evaporated to dryness. The product [$Rh(NNN)(CO)_2$]$_2$ was extracted with hexanes (3 x 10 mL). The three extracts of hexanes were combined, reduced to dryness and redissolved in dry CH_3CN (30 mL). To this solution, [$FeCp_2$][BF_4] (70 mg, 0.26 mmol) was added and the mixture was refluxed for 48 h. The solution was filtered and concentrated to 5 mL. Diethyl ether was added to precipitate the product. Yield: 81 mg, 60%. X-ray quality crystals were obtained by slow diffusion of diethyl ether into an acetonitrile solution of the product. Found: C, 35.71; N, 11.07; H, 3.91 %. Calc. for $C_{40}H_{46}N_{12}B_2F_8Rh_2 \bullet 5CH_2Cl_2 \bullet H_2O$: C, 35.60; N, 11.08; H, 3.85%. δ_H (300 MHz; CD_3CN-d_3) 2.31 (12 H, s, CH_3, tolyl), 2.52 (12 H, s, eq CH_3CN), 7.11 (16 H, m, tolyl-triazenide). $\lambda_{max}(CH_3CN)$/nm 244 (ε x 10^3 /dm^3 mol^{-1} cm^{-1} 19.28), 285 (13.9), ~ 463 (0.8), ~ 534 (0.2). IR (Nujol mull) ν_{CN}/cm^{-1} 2330(m), 2310(m), 2280(w). CV (V, vs Ag/AgCl in ~ 0.10 M [*n*-Bu_4N][PF_6]): $E_{1/2}(red)_1$ -0.35 (quasi-reversible), $E_{1/2}(red)_2$ -1.22, $E_{1/2}(ox)_1$ +1.19, $E_{1/2}(ox)_2$ +1.49.

Preparation of *cis*-[Rh_2(DTolF)$_2$($CNCH_3$)$_6$][BF_4]$_2$ (5). Methyl isocyanide (39 μL, 0.75 mmol) was added to a reddish/brown slurry of *cis*-[Rh_2(DTolF)$_2$(CH_3CN)$_6$][BF_4]$_2$ (80 mg, 0.075 mmol) in CH_3CN (10 mL) which led to a color change to yellow. The solution was stirred under N_2 for 8 h, concentrated to 5 mL and then treated with an excess amount of diethyl ether to induce precipitation of the product. The filtered solid was washed with diethyl ether (3 x 5 mL) and dried overnight under vacuum. Yield 66 mg, 83%. X-Ray quality crystals were obtained by slow diffusion of diethyl ether into a solution of the product in acetonitrile. Found: C, 45.11; N, 12.75; H, 4.26 %. Calc. for $C_{42}H_{48}N_{10}B_2F_8Rh_2$•$CH_3CN$•$CH_2Cl_2$: C, 45.07; N, 12.86; H, 4.46 %. δ_H (300 MHz; CD_3CN-d_3) 2.28 (12 H, s, tolyl CH_3), 2.60 (6 H, s, ax CH_3NC), 3.67 (12 H, s, eq CH_3NC), 7.02 (16 H, m, tolyl), 7.86 (2 H, t, $^3J_{Rh-H}$ = 3 Hz, NCHN). ESI-MS: *m*/*z*: 408.02 for [Rh_2(DTolF)$_2$($CNCH_3$)$_3$]$^{2+}$. λ_{max}(CH_3CN)/nm 267 (ε x 10^3 /dm^3 mol^{-1} cm^{-1} 46.6), ~313 (10.9), ~345 (5), ~392 (1.2), ~425 (0.76). IR (Nujol mull) ν_{NC}/cm^{-1} 2241, 2265(s). CV (V, vs Ag/AgCl in ~ 0.10 M [*n*-Bu_4N][PF_6]): $E_{1/2}$(red)$_1$ -0.67, E(red)$_2$ - 1.20 (irreversible), $E_{1/2}$(ox)$_1$ +1.13, $E_{1/2}$(ox)$_2$ +1.43.

Preparation of *cis*-[Rh_2(F-form)$_2$($CNCH_3$)$_6$][BF_4]$_2$ (6). Methyl isocyanide (48 μL, 0.92 mmol) was added to a reddish/brown slurry of *cis*-[Rh_2(F-form)$_2$(CH_3CN)$_6$][BF_4]$_2$ (100 mg, 0.092 mmol) in CH_3CN (10 mL) which led to the instantaneous formation of a yellow solution which was stirred under N_2 for 12 h to complete the reaction and then concentrated to 5 mL. An excess volume of diethyl ether was added to the solution to induce precipitation of **6**. The resulting solid was washed with diethyl ether (3 x 5 mL) and dried overnight under vacuum to afford the product. Yield 81 mg, 81%. X-Ray quality crystals were obtained by slow diffusion of diethyl ether into a solution of the product in acetonitrile. Found: C, 40.60; N, 12.06; H, 3.19 %. Calc. for $C_{38}H_{36}N_{10}B_2F_{12}Rh_2$•$2H_2O$: C, 40.56; N, 12.46; H, 3.59 %. δ_H (300 MHz; CD_3CN-d_3) 2.74 (6 H, s, ax CH_3NC), 3.68 (12 H, s, eq CH_3NC), 7.04 (16 H, m, *p*-difluorophenyl), 7.84 (2 H, t, $^3J_{Rh-H}$ = 3 Hz, NCHN). ESI-MS: 436.54 for [Rh_2(F-form)$_2$($CNCH_3$)$_4$]$^{2+}$. λ_{max}(CH_3CN)/nm 259 (ε x 10^3 /dm^3 mol^{-1} cm^{-1} 40.9), ~ 318 (11), ~ 340 (4.4), ~ 388 (1.9), ~ 420 (0.8). IR (Nujol mull) ν_{NC}/cm^{-1}

2233(s). CV (V, vs Ag/AgCl in ~ 0.10 M [*n*-Bu_4N][PF_6]): $E_{1/2}(red)_1$ -0.61, $E(red)_2$ - 1.09 (irreversible), $E_{1/2}(ox)_1$ +1.32, $E(ox)_2$ +1.70 (irreversible).

Preparation of *cis*-[$Rh_2(NNN)_2(CNCH_3)_6$][BF_4]$_2$ (7). The addition of methyl isocyanide (38 μL, 0.73 mmol) to a reddish/brown slurry of *cis*-[$Rh_2(NNN)_2(CH_3CN)_6$][BF_4]$_2$ (78 mg, 0.073 mmol) in CH_3CN (10 mL) led to an immediate color change to yellow. The solution was stirred under N_2 for 12 h and concentrated to 5 mL. Excess diethyl ether was added to the solution to induce precipitation of the product which was collected, washed with diethyl ether (3 x 5 mL) and dried overnight under vacuum to afford **7**. Yield 66 mg, 85%. X-Ray quality crystals were obtained by slow diffusion of diethyl ether into a solution of the product in acetonitrile. Found: C, 36.34; N, 12.44; H, 4.13 %. Calc. for $C_{46}H_{55}B_2F_8N_{15}Rh_2$•$6CH_2Cl_2$: C, 36.56; N 12.31; H, 3.96 %. δ_H (300 MHz; CD_3CN-d_3) 2.31 (12 H, s, tolyl CH_3), 2.73 (6 H, s, ax CH_3NC), 3.66 (12 H, s, eq CH_3NC), 7.10 (16 H, m, tolyl-triazenide). ESI-MS: $[Rh_2(NNN)_2(CNCH_3)_3]^{2+}$, 408.02. $\lambda_{max}(CH_3CN)$/nm 232 (ε x 10^3 /dm^3 mol^{-1} cm^{-1} 18.3), 284 (11), 389 (1.4), ~450 (0.3). IR (Nujol mull) ν_{NC}/cm^{-1} 2244(s). CV (V, glassy carbon working electrode in ~ 0.10 M [*n*-Bu_4N][PF_6]): $E(red)_1$ -0.58 (irreversible), $E_{1/2}(red)_2$ - 1.18 (quasi-reversible), $E_{1/2}(ox)_1$ +1.28, $E_{1/2}(ox)_2$ +1.50.

Preparation of *cis*-[$Rh_2[Ph_2P(C_6H_4)]_2(CNCH_3)_6$][$BF_4$]$_2$ (8). Methyl isocyanide (45 μL, 0.86 mmol) was added to a solution of *cis*-[$Rh_2[Ph_2P(C_6H_4)]_2(CH_3CN)_6$][$BF_4$]$_2$ (85 mg, 0.074 mmol) in CH_3CN (5 mL) which led to a color change from reddish-yellow to light yellow. The reaction mixture was stirred for 30 min under N_2 and treated with diethyl ether which led to precipitation of the desired product Yield 75 mg, 88 %. X-ray quality crystals were obtained by slow diffusion of diethyl ether into an acetonitrile solution of the product in the dark. Found: C, 48.78; N, 7.22; H, 4.07 %. Calc. for $C_{48}H_{46}N_6B_2F_8P_2Rh_2$•$2H_2O$: C, 48.64; N 7.10; H, 4.26 %. δ_H (300 MHz; CD_3CN-d_3) 2.50 (6 H, s, ax CH_3NC), 3.27 (6 H, s, eq CH_3NC, *trans* to C), 3.48 (6 H, s, eq CH_3NC, *trans* to P), 6.70-7.70 ppm (28 H, m, $Ph_2P(C_6H_4)$). δ^{31}_P (300 MHz; CD_3CN-d_3; H_3PO_4) 20.94 ($^1J_{Rh\text{-}P}$=101.5 Hz). ESI-MS: {[$Rh_2[Ph_2P(C_6H_4)]_2(CNCH_3)_6$][$BF_4$]}$^+$ 1061.16; {[$Rh_2[Ph_2P(C_6H_4)]_2(CNCH_3)_5$][$BF_4$]}$^+$ 1020.13; {[$Rh_2[Ph_2P(C_6H_4)]_2(CNCH_3)_5$][$BF_4$]}$^+$ 979.11. $\lambda_{max}(CH_3CN)$/nm 204 (ε x 10^3 /dm^3 mol^{-1} cm^{-1} 120), 273 (14), ~290 (11), 362 (10). IR (Nujol

mull) ν_{NC}/cm^{-1} 2219(s). CV (V, vs Ag/AgCl in ~ 0.10 M [*n*-Bu_4N][PF_6]): E(red) -1.38 (irreversible), $E_{1/2}$(ox) +1.23.

Discussion

Syntheses. Compounds **1**-**3** were prepared by oxidation of Rh(I) starting materials; **1** and **2** were synthesized by similar procedures whereas [Rh(F-form)(COD)]$_2$, which is a precursor to **2**, was synthesized according to a method similar to [Rh(DTolF)(COD)]$_2$.[3] Subsequently, [Rh(F-form)(COD)]$_2$ was treated with an excess of $AgBF_4$[5] to afford **2** (Eq. 1):

$$[\text{Rh(F-form)(COD)}]_2 \xrightarrow[\text{CH}_2\text{Cl}_2/\text{CH}_3\text{CN}\ \text{r.t.}]{\text{AgBF}_4} \underset{\mathbf{2}}{\textit{cis}\text{-}[\text{Rh}_2(\text{F-form})_2(\text{CH}_3\text{CN})_6][\text{BF}_4]_2} \qquad \textbf{Eq. 1}$$

The compound [Rh(NNN)$(CO)_2]_2$, which is a precursor to **3**, was prepared by a slightly modified published procedure[4] as shown in Eq. 2. A slight excess of [$FeCp_2$][BF_4] was used to oxidize Rh(I) to Rh(II) to afford **3** and ferrocene.

$$[\text{RhCl(CO)}_2]_2 \xrightarrow[\text{CH}_2\text{Cl}_2]{\text{NNHN, NEt}_3} [\text{Rh(NNN)(CO)}_2]_2 \xrightarrow[\text{CH}_3\text{CN}]{[\text{Fe(Cp)}_2][\text{BF}_4]} \underset{\mathbf{3}}{\textit{cis}\text{-}[\text{Rh}_2(\text{NNN})_2(\text{CH}_3\text{CN})_6][\text{BF}_4]_2} \qquad \textbf{Eq. 2}$$

The corresponding methyl isocyanide analogs **5**-**8** were prepared by substitution of the monodentate acetonitrile ligands with methyl isocyanide in **1**-**4**. An excess of CH_3NC was used during the syntheses of the methyl isocyanide analogs **5**-**8**. The general synthetic route for **5**-**7** is depicted in Eq. 3:

$$\textit{cis}\text{-}[\text{Rh}_2(\text{N-N})_2(\text{CH}_3\text{CN})_6][\text{BF}_4]_2 \xrightarrow[\text{CH}_3\text{CN}\ \text{r.t.}]{\text{10 equ. CH}_3\text{NC}} \textit{cis}\text{-}[\text{Rh}_2(\text{N-N})_2(\text{CNCH}_3)_6][\text{BF}_4]_2 \qquad \textbf{Eq. 3}$$

A characteristic color change occurs from reddish/brown to light yellow upon addition of methyl isocyanide to solutions of **1**-**3** to afford **5**-**7**, respectively. Unlike compounds **5**-**7**, prolonged stirring of **8** in CH_3CN leads to product decomposition as evidenced by ^{1}H-NMR spectroscopy (*vide infra*) therefore **8** was prepared by stirring **4** under N_2 for 30 min only, in the presence of CH_3NC.

NMR Spectroscopic Studies. Compounds **1**-**8** were characterized by ^{1}H-NMR spectroscopy and the exchange process of the monodentate ligands with the deuterated solvent (CD_3CN) was monitored. In the aromatic region of the ^{1}H-NMR spectra for **1**-**2** and **5**-**6**, the characteristic triplet resonances attributed to the N-CH-N groups of the formamidinate ligands appear at δ 7.5-7.9 ppm with coupling constants $^{3}J_{Rh\text{-}H}$(N-CH-N) ~ 3-4 Hz.[5] For compound **3**, the multiplet at δ 7.11 ppm arises from the phenyl protons of the bridging $[NNN]^-$ ligands, whereas for **1** and **2**, the formamidinate phenyl ^{1}H-NMR resonances appear at δ ~ 7.0 ppm. The strong *trans* effect of the electron-donating bridging ligands in **1**-**3**, leads to an increased lability of the *trans* eq CH_3CN ligands.[6] The latter was confirmed by the gradual decrease of the resonance intensity corresponding to the eq CH_3CN ligands (δ ~2.50 ppm for **1**-**3**) with a concomitant increase of the intensity for the free CH_3CN resonance (δ 1.96 ppm for **1**-**3**) in the aliphatic region of the ^{1}H-NMR spectrum of each complex in CD_3CN. Despite the slower eq CH_3CN/CD_3CN exchange rate for **2** and **3** as compared to **1**, complete exchange takes place in less than 6 h (e.g., Fig. S1, ESI for **2**). Conversely, the intensity of the resonances attributed to the ax (δ ~ 2.73 ppm) and eq (δ ~3.66 ppm) CH_3NC groups, in the ^{1}H NMR spectra of **5**-**7** in CD_3CN do not decrease with time, i.e., no exchange of the CH_3NC groups with the bulk CD_3CN solvent is observed after one week (e.g., Fig. S2, ESI for **5**). The latter observation is attributed to the better σ-donating and π-accepting abilities of CH_3NC as compared to CH_3CN, which lead to stronger Rh-C bonds with the dirhodium core in **5**-**7**.

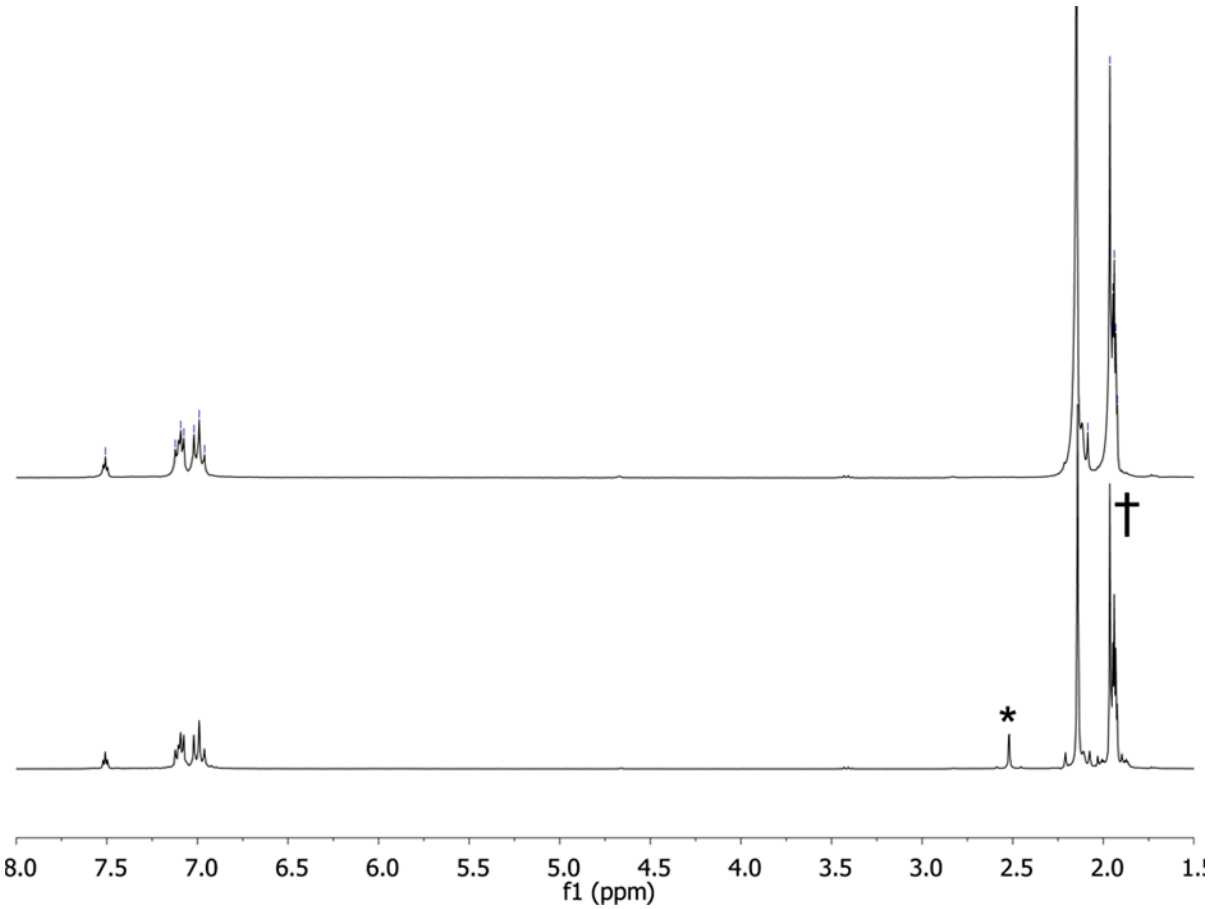

Fig. S1 ^{1}H-NMR spectra for **2** in CD_3CN at different time intervals. (*: eq CH_3CN, †: free CH_3CN) Lower spectrum: 10 minutes after dissolution of **2**. Upper spectrum: 6 hours after dissolution of **2**.

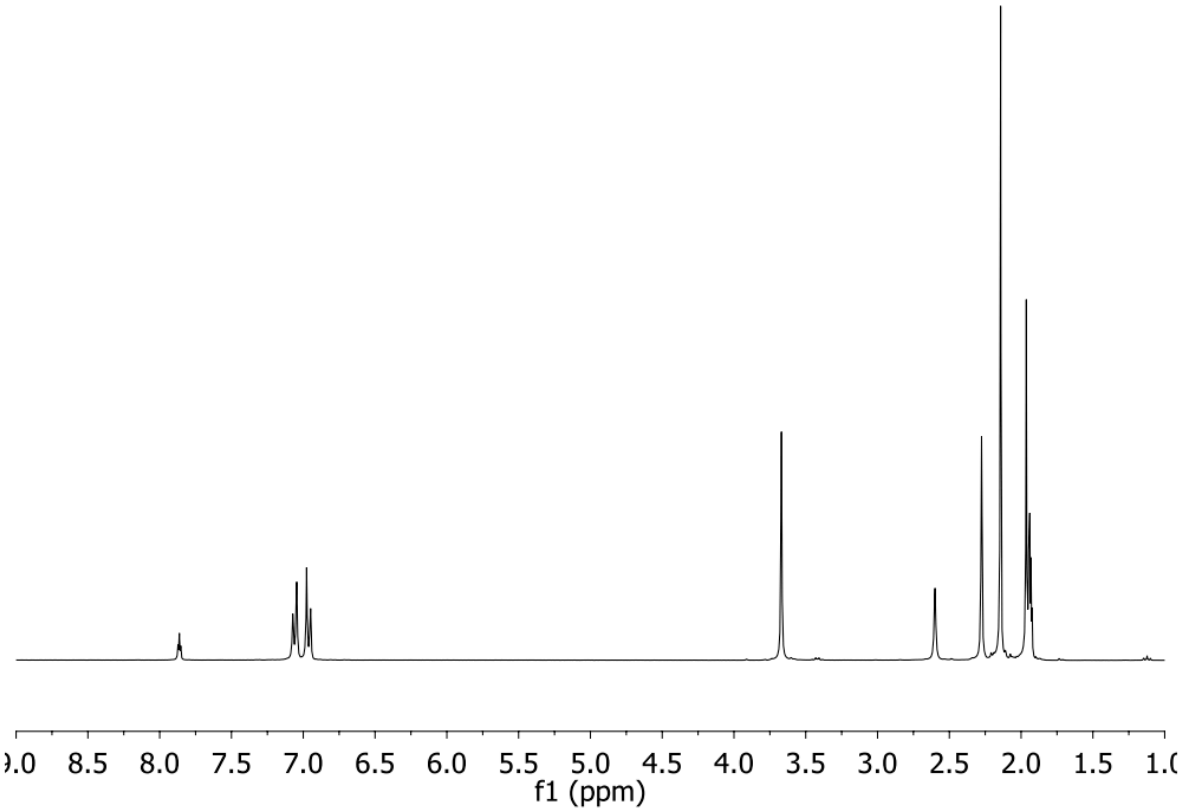

Fig. S2 ^{1}H-NMR spectrum of **5** in CD_3CN recorded 10 min after dissolution with no changes being observed after one week in solution.

NMR of Compound 8. The X-ray crystallographic data for the orthometalated compounds **4** and **8** revealed racemic mixtures of the *R* and *S* isomers; the Rh centers are supported by two *cis* $[Ph_2P(C_6H_4)]^-$ groups in a head-to-tail orientation. As evidenced by the ^{1}H-NMR spectra, both isomers exhibit the same chemical shifts due to fast rotation of the molecules in solution. The presence of only one resonance for CH_3CN in the ^{1}H-NMR spectrum of **4**, within 10 min of dissolution, indicates fast exchange of the eq CH_3CN ligands with the solvent (CD_3CN), due to the strong σ-donating ability of the bridging phosphine ligands.[7,8] In contrast, due to the decreased lability of CH_3NC, as compared to CH_3CN, and the asymmetry of the bridging ligands, the ^{1}H-NMR spectrum of **8** displays three CH_3NC resonances at δ 3.48, 3.27 and 2.50 ppm, in a 1:1:1 ratio (Fig.

S3, ESI), which correspond to eq CH_3NC *trans* to the P and C atoms as well as the ax CH_3NC groups, respectively. Monitoring **8** by ^1H NMR spectroscopy in CD_3CN, however, revealed slow decomposition as indicated by the disappearance of the three aforementioned CH_3NC resonances at the same rate and the concomitant appearance of a new resonance at δ 3.38 ppm in the ^1H NMR spectra (Fig. S3, ESI). The $^{31}P\{^1H\}$ NMR spectrum of **8** exhibits a doublet at δ ~ 21 ppm ($^1J_{Rh\text{-}P}$ = 101.5 Hz) with the characteristic ^{102}Rh-^{31}P coupling;[9] the doublet decreases in intensity and after 12 h, new resonances appear in the spectrum, and increase in intensity with time (Fig. S4, ESI; spectra at 12 h and 4 days). The instability of **8** in solution as a function of time, indicated by the NMR data, is also corroborated by the fragmentation pattern that **8** exhibits in the MS studies. On the contrary, the ESI-MS data for **2**-**7** show the main peaks corresponding to the parent species with a 2^+ charge and the appropriate isotopic distributions. Sequential loss of the monodentate ligands, either CH_3CN or CH_3NC, is observed in the ESI-MS of **2**-**7**.

Fragments for compound 8 found in ESI-MS analysis: $[Rh_2\{Ph_2P(C_6H_4)\}_2]^{2+}$, 366.00; $[Rh_2\{Ph_2P(C_6H_4)\}_2(CNCH_3)]^{2+}$, 384.51; $[Rh_2\{Ph_2P(C_6H_4)\}_2(CNCH_3)_2]^{2+}$, 405.00; $[Rh_2\{Ph_2P(C_6H_4)\}_2(CNCH_3)_3]^{2+}$, 425.51; $[Rh_2\{Ph_2P(C_6H_4)\}_2(CNCH_3)_4]^{2+}$, 446.03; $[Rh_2\{Ph_2P(C_6H_4)\}_2(CNCH_3)_5]^{2+}$, 466.56; $[Rh\{Ph_2P(C_6H_4)\}_2]+H^+$, 625.07; $[Rh\{Ph_2P(C_6H_4)\}_2(CNCH_3)]+H^+$, 666.09; $[Rh\{Ph_2P(C_6H_4)\}_2(CNCH_3)_2]+H^+$, 707.13; $[Rh_2\{PPh_2P(C_6H_4)\}_2(CNCH_3)_3](BF_4)^+$, 938.08; $[Rh_2\{Ph_2P(C_6H_4)\}_2(CNCH_3)_4](BF_4)^+$, 979.11; $[Rh_2\{Ph_2P(C_6H_4)\}_2(CNCH_3)_5](BF_4)^+$, 1020.13; $[Rh_2\{Ph_2P(C_6H_4)\}_2(CNCH_3)_6](BF_4)^+$, 1061.16.

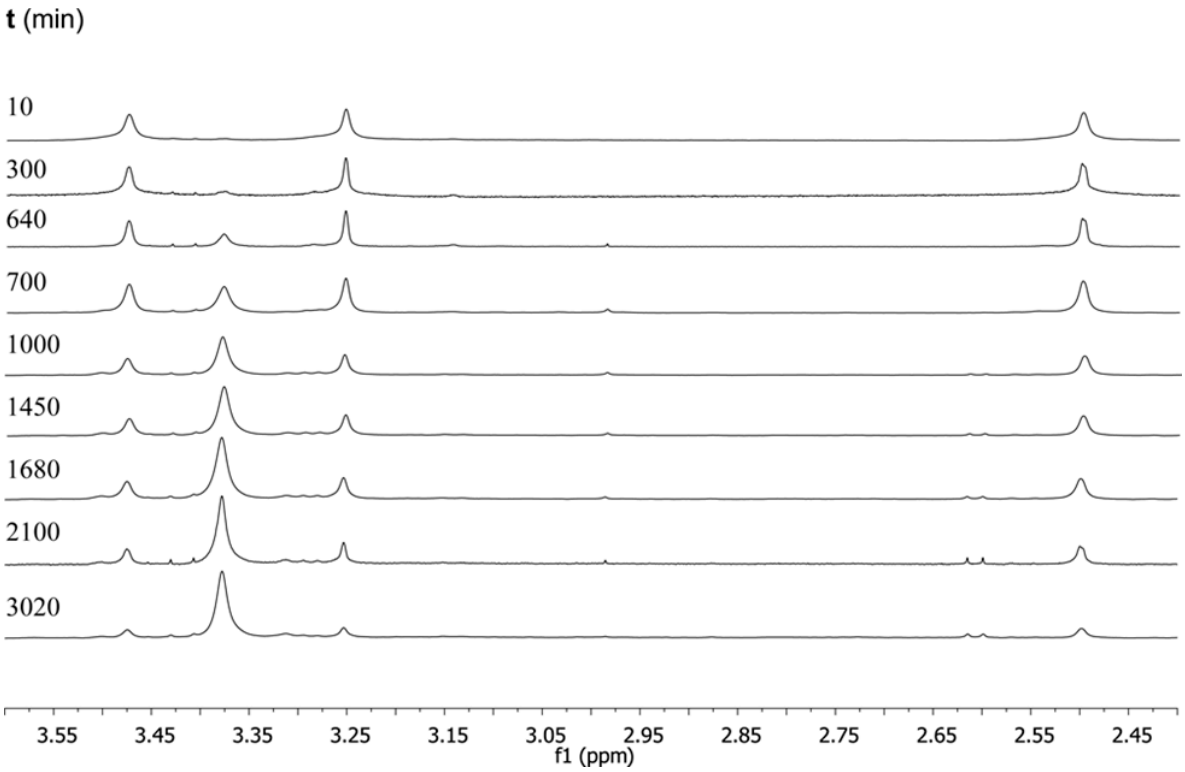

Fig. S3 Aliphatic region of the ^{1}H-NMR spectra for **8** in CD_3CN at different time intervals (in min).

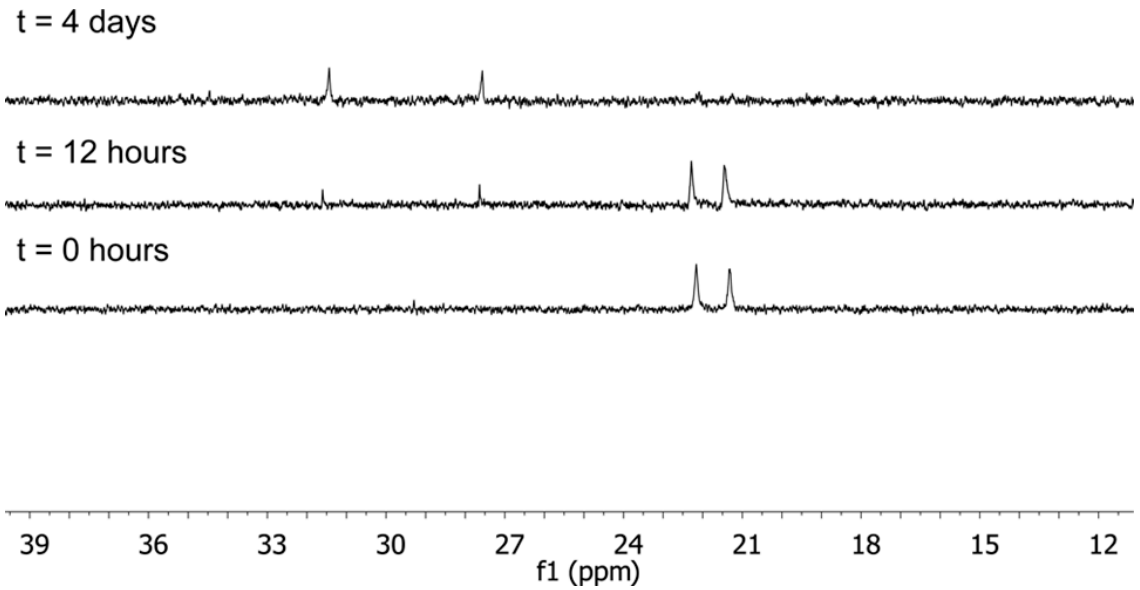

Fig. S4 ^{31}P $\{^{1}H\}$-NMR spectra of **8** in CD_3CN obtained at different time intervals. Spectra are referenced to 30% H_3PO_4 in D_2O (0 ppm).

X-Ray Crystallographic Studies. X-ray data sets for **2**, **3** and **5**-**8** were collected on a Bruker CCD APEX diffractometer equipped with a graphite monochromated MoK_a radiation source ($\lambda = 0.71073$ Å). A hemisphere of crystallographic data was collected by a combination of four sets of exposure. Each set had a different ϕ angle for the crystals, and each exposure covered 0.3° in ω. The exposure time for **5**-**8** was 10s whereas for **2**, **3**, it was 20s. Crystal decay was monitored by analyzing duplicate reflections and was found to be less than 1%, therefore no decay correction was applied. The frames were integrated with the Bruker AXS SAINT Software package,[10] and the data were corrected for absorption using the SADABS program in the same software package.[11] The structures were solved by direct methods and refined by using X-SEED,[12] a graphical interface to the SHELX97 suite of programs.[13] In the final cycles of the refinement, all atoms except for hydrogen were refined anisotropically.

Refinement of X-Ray Crystallographic Structures. Hydrogen atoms on the phenyl rings were placed in geometrically optimized positions, and the bond distances and angles were idealized during refinement with the hydrogen U values set at 1.2 times the equivalent isotropic U of the C atoms to which they were attached. The hydrogen atoms on methyl groups were set at the positions with the maximum electron density during the refinement, with the hydrogen U value set at 1.5 times the equivalent isotropic U of the C atom that they were attached.

Table 1 (Complete). Crystal and structural refinement data for **2**•Et_2O, **3**, **5**.

	2•Et_2O	**3**	**5**
Formula	$C_{42}H_{46}N_{10}F_{12}B_2ORh_2$	$C_{40}H_{46}N_{12}B_2F_8Rh_2$	$C_{42}H_{48}N_{10}B_2F_8Rh_2$
Formula weight	1162.31	1074.30	1072.33
Temperature/ K	110(2)	110(2)	110(2)
Crystal system	Monoclinic	Orthorhombic	Orthorhombic
Space group	$P2_1/c$	$Pbca$	$Pbca$
a, b, c/ Å	11.042(2), 32.589(7), 14.243(3)	14.135(3), 21.331(4), 31.170(6)	14.338(3), 21.619(4), 31.136(6)
α, β, γ/ º	90, 100.66(3), 90	90, 90, 90	90, 90, 90
V/ Å^3	5036.5(17)	9399(3)	9651(3)
Crystal description, color	red plate	red block	yellow plate
Crystal size/ mm^3	0.04 x 0.08 x 0.10	0.08 x 0.10 x 0.13	0.02 x 0.06 x 0.25
Z	4	8	8
$D_{calc.}$/g/cm^3	1.5314	1.5183	1.4758
μ / mm^{-1}	0.74	0.78	0.76
F(000)	2336.0	4336.0	4336
2θ range for data collection/º	53.62	41.63	57.24
Diffraction limits (h, k, l)	-13 ≤ h ≤ 13 -41 ≤ k ≤ 41 -17 ≤ l ≤ 17	-14 ≤ h ≤ 14 -21 ≤ k ≤ 21 -31 ≤ l ≤ 31	-18 ≤ h ≤ 19 -29 ≤ k ≤ 28 -41 ≤ l ≤ 39
Reflections measured	54314	57506	105468
Independent reflections	R(int) = 0.0635	R(int) = 0.0248	R(int) = 0.0301
Completeness to θ max/%	99.3	99.9	95.4
Data/restraints/parameters	10690/0/630	4201 /12/588	11808/0/587
R_1,[a] wR_2[b] [I >2σ(I)]	R = 0.0587, wR = 0.1314	R = 0.059, wR = 0.1570	R = 0.0262, wR = 0.0590
R_1,[a] wR_2[b] (all data)	R = 0.0852, wR = 0.1435	R = 0.0677, wR = 0.1719	R = 0.0374, wR = 0.0660
Goodness-of-fit parameter (all data)[c] (F^2)	1.052	1.193	1.059
Largest diff. peak and hole/ e.Å^{-3}	0.91/-0.93	0.88/-0.65	0.83/-0.62

Table 1 (continued-complete). Crystal and structural refinement data for **6**•Et_2O, **7**, **8**.

	6•Et_2O	**7**	**8**
Formula	$C_{42}H_{46}N_{10}F_{12}B_2ORh_2$	$C_{40}H_{46}N_{12}B_2F_8Rh_2$	$C_{96}H_{92}N_{12}P_4B_4F_{16}Rh_4$
Formula weight	1162.31	1074.30	2296.60
Temperature/ K	110(2)	110(2)	110(2)
Crystal system	Monoclinic	Orthorhombic	Monoclinic
Space group	$P2_1/c$	$Pbca$	$Pbca$
a, b, c/ Å	11.110(2), 31.777(6), 14.195(3)	14.126(3), 21.399(4), 31.434(6)	22.272(4), 22.161(4), 22.409(4)
α, β, γ/ º	90, 101.13(3), 90	90, 90, 90	90, 119.43(3), 90
V/ Å^3	4917.3(17)	9502(3)	9633(3)
Crystal description, color	Yellow block	Yellow plate	Yellow block
Crystal size/ mm^3	0.05 x 0.10 x 0.11	0.13 x 0.10 x 0.03	0.16 x 0.12 x 0.11
Z	4	8	4
$D_{calc.}$/ g/cm^3	1.5698	1.5017	1.5833
μ / mm^{-1}	0.76	0.77	0.82
F(000)	2336	4336.0	4624
2θ range for data collection/º	50.02	49.46	54.64
Diffraction limits (h, k, l)	-13 ≤ h ≤ 13 -37 ≤ k ≤ 37 -16 ≤ l ≤ 16	-16 ≤ h ≤ 16 -25 ≤ k ≤ 25 -36 ≤ l ≤ 36	-28 ≤ h ≤ 28 -28 ≤ k ≤ 28 -28 ≤ l ≤ 28
Reflections measured	44350	83459	107654
Independent reflections	R(int) = 0.0359	R(int) = 0.0885	R(int) = 0.0443
Completeness to θ max/%	100	100	99.5
Data/restraints/parameters	8664/ 0/630	8110/0/587	21603/0/1256
R_1,[a] wR_2[b] [$I > 2\sigma(I)$]	R = 0.0374, wR = 0.0914	R = 0.0443, wR = 0.1010	R = 0.0328, wR = 0.0899
R_1,[a] wR_2[b] (all data)	R = 0.0480, wR = 0.0981	R = 0.0680, wR = 0.1133	R = 0.0459, wR = 0.0978
Goodness-of-fit parameter (all data)[c]	1.038	1.019	1.060
Largest diff. peak and hole/ e.Å^{-3}	1.08/-0.66	1.08/-1.09	0.62/-0.78

[a] $R = \Sigma \left| \left| F_o \right| - \left| F_c \right| \right| / \Sigma \left| F_o \right|$. [b] $wR = \{\Sigma [w(F_o^2 - F_c^2)^2] / \Sigma w(F_o^2)^2]\}^{1/2}$. [c] Goodness-of-fit = $\{\Sigma [w(F_o^2 - F_c^2)^2] / (n-p)\}^{1/2}$, where n is the number of reflections and p is the total number of parameters refined.

***cis*-[Rh$_2$(F-form)$_2$(CH$_3$CN)$_6$)][BF$_4$]$_2$•Et$_2$O (2•Et$_2$O), (2).** A thermal ellipsoid plot of the cationic unit in **2** is shown in Fig. S5. The dirhodium unit is bridged by two [F-form]$^-$ ligands in a *cis* arrangement with six CH$_3$CN ligands occupying the remaining Rh(II) coordination sites. The Rh-Rh bond distance is 2.571(1) Å which is comparable to **1** and the compounds *cis*-[Rh$_2$(DTolF)$_2$(bpy)(CH$_3$CN)$_3$][BF$_4$]$_2$ and *cis*-[Rh$_2$(DTolF)$_2$(bpy)$_2$(CH$_3$CN)][BF$_4$]$_2$.[6] The Rh-N [F-form]$^-$ and Rh-N (eq CH$_3$CN) distances are in the ranges 2.024(4)-2.052(5) and 2.032(5)-2.043(5) Å, respectively. The previous distances are similar to **1** but longer than the corresponding distances in *cis*-[Rh$_2$(O$_2$CCH$_3$)$_2$(CH$_3$CN)$_6$][BF$_4$]$_2$.[14] As in the case of **1** and *cis*-[Ir$_2$(DTolF)$_2$(CH$_3$CN)$_6$][BF$_4$]$_2$,[15] a splaying of the four eq CH$_3$CN ligands occurs. The [F-form]$^-$ groups are twisted by 18.0(2)° from the eclipsed conformation and the eq CH$_3$CN groups are twisted by 22.8(2)° due to the steric constraints imposed by the bridging ligands.

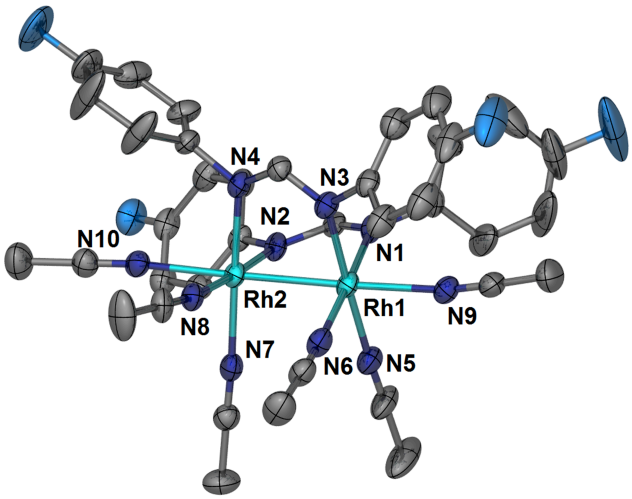

Fig. S5 Thermal ellipsoid plot for the cationic unit in **2** at 50% probability level. Selected bond distances (Å) and angles (°): Rh1-Rh2 2.571(1), Rh1-N9 2.251(4), Rh1-N1 2.038(5), Rh1-N5 2.032(5), Rh1-N6 2.040(5), Rh2-N2 2.046(5) , Rh2-N4 2.024(4). Colors for thermal ellipsoids: C: gray, N: dark blue, F: light blue, Rh: teal.

***cis*-[Rh$_2$(NNN)$_2$(CH$_3$CN)$_6$][BF$_4$]$_2$, (3).** The cationic unit in **3** is shown in Fig. S6. The Rh-Rh bond distance is 2.5135(9) Å, which is slightly shorter than the Rh-Rh distance in *cis*-[Rh$_2$(NNN)$_2$(CH$_3$CN)$_3$(bpy)][PF$_6$]$_2$[16] (2.534(2) Å). The Rh-N (eq CH$_3$CN) bond distances are in

the range 1.996(7)-2.024(6) Å and are comparable to the corresponding distances in **1**, **2** and *cis*-$[Rh_2(NNN)_2(CH_3CN)_3(bpy)][PF_6]_2$.[16] The Rh-N triazenide bond distances are in the range 2.011(6)-2.024(6) Å, and are slightly shorter than the corresponding ones in **1**, **2** and Rh-N (N *trans* to eq bpy in $[NNN]^-$) and comparable to the Rh-N ($[NNN]^-$, *trans* to eq CH_3CN) in *cis*-$[Rh_2(NNN)_2(CH_3CN)_3(bpy)][PF_6]_2$. The eq CH_3CN groups and the bridging ligands ($[NNN]^-$) are twisted by ~23.0° and ~20.3°, respectively, from the eclipsed configuration.

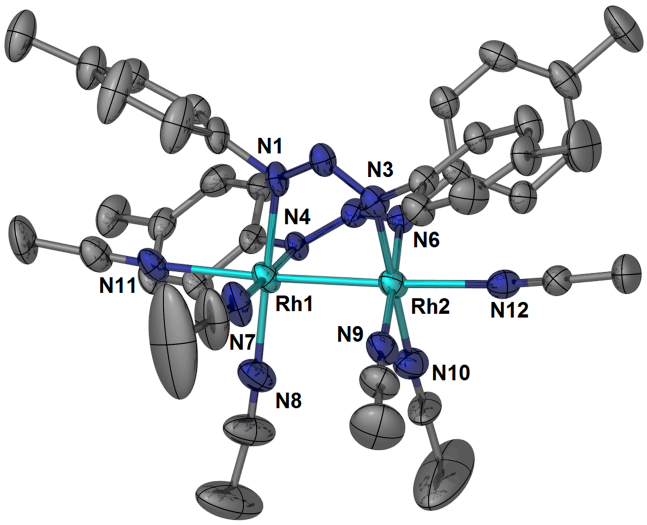

Fig S6. Thermal ellipsoid plot for the cationic unit in **3** at 50% probability level. Selected bond distances (Å) and angles (°): Rh2-Rh1 2.5135(9), Rh2-N12 2.202(7), Rh2-N6 2.011(6), Rh2-N10 1.996(7), Rh2-N9 2.024(6), Rh1-N4 2.023(6), Rh1-N11 2.225(7), Rh1-N1 2.024(6), Rh1-N7 2.007(8). Colors for thermal ellipsoids: C: gray, N: dark blue, Rh: teal.

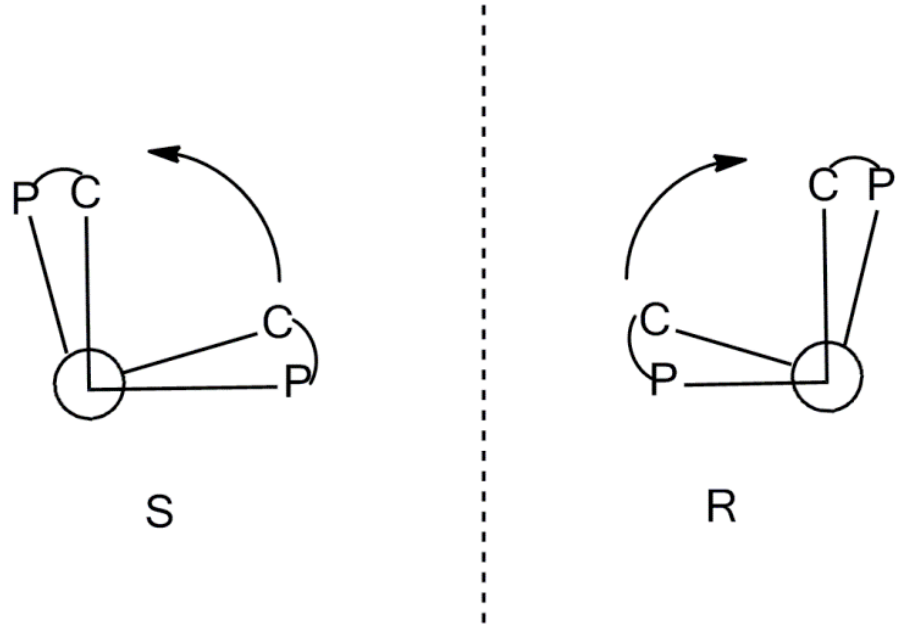

Scheme S1. *R* and *S* enantiomers of dirhodium orthometalated phosphine complexes.[7,17,18]

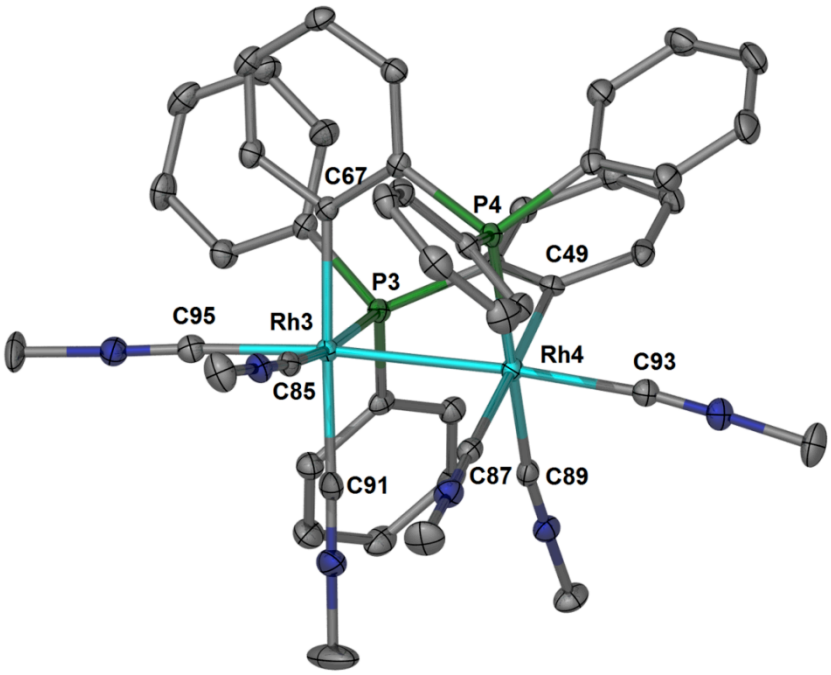

Fig. S7 Thermal ellipsoid plot of **8**-*R* at the 50% probability level. All the hydrogen atoms and the anions have been omitted for clarity. Selected bond distances (Å), angles (º) and dihedral angles (º): Rh3-Rh4 2.766(1), Rh3-P3 2.3056(8), Rh3-C67 2.099(3), Rh3-C95 2.033(3), Rh3-

C85 2.005(3), Rh3-C91 2.011(3), Rh4-P4 2.3076(8), Rh4-C49 2.096(3), Rh4-C87 2.019(3), Rh4-C89 2.004(3), Rh4-C93 2.040(2), Rh4-Rh3-C95 174.50(8), Rh3-Rh4-C93 175.20(8), Rh4-C89-N9 172.5(2), Rh4-C93-N12 171.9(2), Rh4-C87-N10 175.9(3), Rh3-C95-N11 173.7(3), Rh3-C85-N8 173.1(2), Rh3-C91-N7 177.3(3), C67-Rh3-Rh4-P4 21.08(8), P3-Rh3-Rh4-C49 21.19(8), C85-Rh3-Rh4-C487 30.7(1), C91-Rh1-Rh2-C89 31.8(1).

Structural Details about *cis*-$[Rh_2[Ph_2P(C_6H_4)]_2(CNCH_3)_6][BF_4]_2$, (8). The Rh-P bond lengths (2.30 Å) for both isomers of **8** are ~0.10 Å longer than Rh-P in *cis*-$[Rh_2[Ph_2P(C_6H_4)]_2(O_2CCH_3)_2]\bullet 2CH_3CO_2H$ and *cis*-$[Rh_2(O_2CCH_3)_2[Ph_2P(C_6H_4)]_2]\bullet 2C_5H_5N$,[7] and ~0.05 Å longer than in **4**. The Rh-C bond lengths (2.07 Å; bridging phosphine) in **8** are ~0.07 Å longer than the corresponding distances in *cis*-$[Rh_2[Ph_2P(C_6H_4)]_2(O_2CCH_3)_2]\bullet 2CH_3CO_2H$, *cis*-$[Rh_2(O_2CCH_3)_2[Ph_2P(C_6H_4)]_2]\bullet 2C_5H_5N$ and **4**,[7,18]which is attributed to the strong *trans* influence of the Rh-C (eq $CNCH_3$) bonds on the bridging orthometalated ligands (Table 6 of main paper). The bridging phosphine groups exhibit considerably smaller twist angles from an eclipsed conformation than the CH_3NC groups, with dihedral angles -21.29(8)° and -20.47(8)° in **8**-*S*. Likewise, for **8**-*R*, they are 21.08(8)° and 21.19(8)°. These distortions are similar to those encountered in **4**, but larger than the angles in *cis*-$[Rh_2[Ph_2P(C_6H_4)]_2(O_2CCH_3)_2]\bullet 2CH_3CO_2H$, wherein the acetate bridging groups are twisted by ~ 12.22° from the eclipsed conformation.

Computational Studies. DFT calculations were performed on the cationic units of **1**-**8** in an attempt to gain further insight into their structural, electrochemical and electronic absorption properties. The graphical representations of the optimized structures are shown in Fig. S8; detailed structural parameters are listed in Table S1. In general, the good agreement of the bond lengths and angles with the X-ray data indicates that the level of theory and the basis sets that were used are reliable. The structural parameters of the optimized metal complexes closely resemble those experimentally found by X-ray crystallography. In **1**-**3**, the Rh-Rh bond distances in the cationic units are ~ 0.09 Å shorter than the distances in **5**-**7**. Moreover, a significant decrease of the Rh-L bond distances (L monodentate ligand, L: CH_3CN in **1**-**3**, L: CH_3NC in **5**-**7**) was also successfully predicted by the calculations for the pairs **1**/**5**, **2**/**6, 3**/**7**. The Rh-Rh bond distance in the optimized cationic unit of **4** is comparable to the crystal structure, whereas in **8**, it

is by ~ 0.05 Å longer than the experimentally determined value. In **4**, slightly longer Rh-N bond distances (eq CH_3CN, *trans* to C) than the Rh-N bond distances (eq CH_3CN *trans* to P) were also successfully predicted, indicating the stronger *trans* influence imposed by the Rh-C bond. For **8**, the Rh-C (ax $CNCH_3$) and Rh-C (eq $CNCH_3$) bond distances are very similar, in agreement with the X-ray diffraction data. The calculated dihedral angles ω for **1**-**8**, defined by the equatorial ligands and the two Rh centers, are slightly higher than those in the crystal structures but within a similar range.

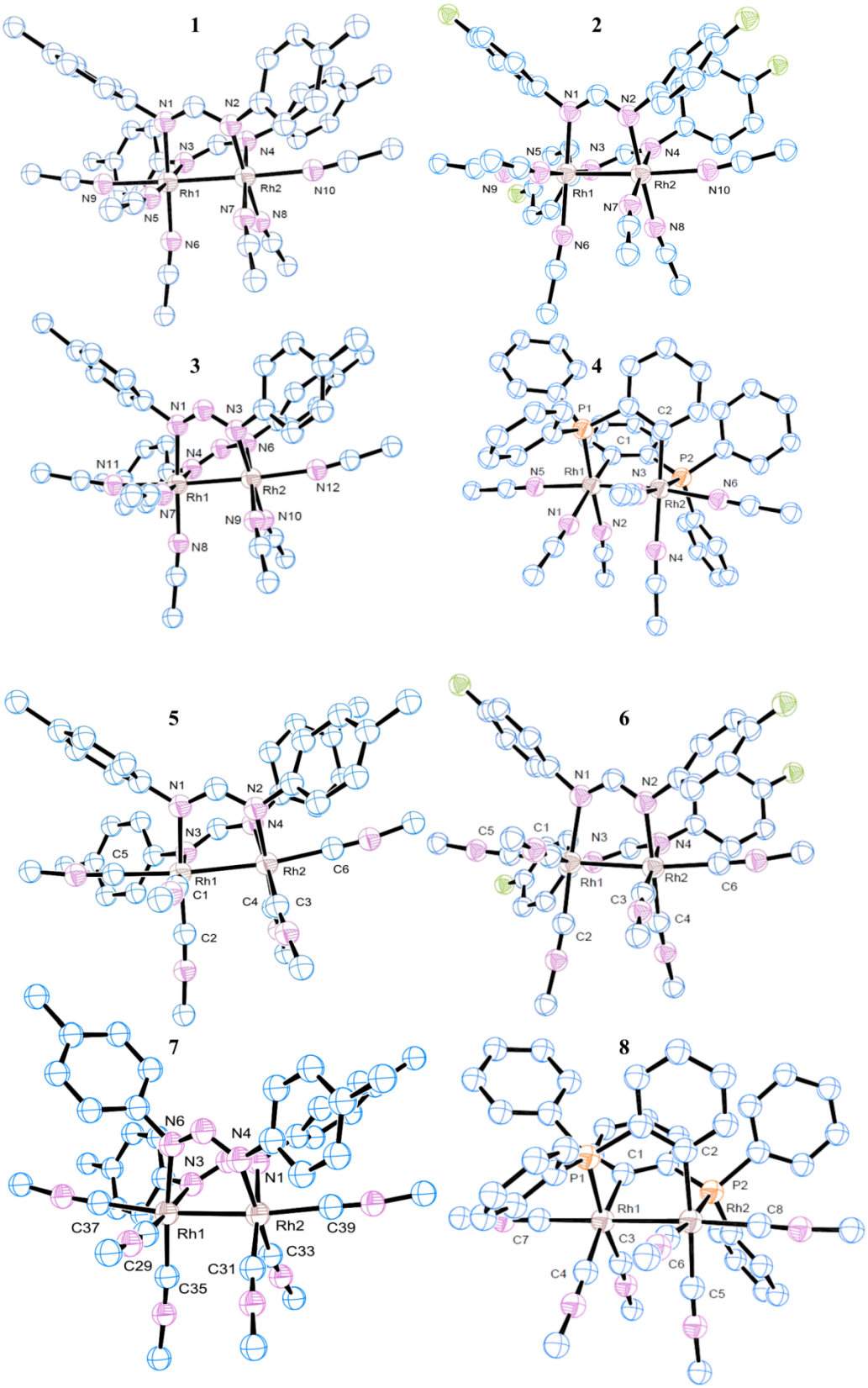

Fig. S8 Gas phase optimized structures for **1**-**8**.

Table S1. Important bond distances (Å) and dihedral angles (º) for the optimized (with the solvation model in CH_3CN) and crystallographically determined structures of **1**-**8**.

1	**Calculated**	**X-ray Data**
	Bond distances (Å)	**Bond distances (Å)**
Rh1-Rh2	2.5759	2.5653(7)
Rh1-N1	2.0396	2.020(4)
Rh1-N3	2.0444	2.029(5)
Rh2-N2	2.0439	2.043(4)
Rh2-N4	2.0383	2.043(5)
Rh1-N5	2.0428	2.023(5)
Rh1-N6	2.0479	2.030(5)
Rh2-N7	2.0487	2.020(5)
Rh2-N8	2.0433	2.024(5)
Rh1-N9	2.2183	2.214(6)
Rh2-N10	2.2183	2.247(5)
	Dihedral angles (º)	**Dihedral angles** (º)
N1-Rh1-Rh2-N2	18.122	18.2(2)
N3-Rh1-Rh2-N4	18.110	18.4(2)
N5-Rh1-Rh2-N7	26.633	21.3(2)
N6-Rh1-Rh2-N8	26.589	22.5(2)
2	**Calculated**	**X-ray Data**
	Bond distances (Å)	**Bond distances (Å)**
Rh1-Rh2	2.5688	2.571(1)
Rh1-N1	2.0462	2.038(5)
Rh1-N3	2.0484	2.052(5)
Rh2-N2	2.0337	2.046(5)
Rh2-N4	2.0340	2.024(4)
Rh1-N5	2.0411	2.032(5)
Rh1-N6	2.0463	2.040(5)
Rh2-N7	2.0512	2.043(5)
Rh2-N8	2.0472	2.034(5)
Rh1-N9	2.2191	2.251(4)
Rh2-N10	2.2311	2.195(4)
	Dihedral angles (º)	**Dihedral angles** (º)
N1-Rh1-Rh2-N2	20.714	18.0(2)
N3-Rh1-Rh2-N4	21.659	18.0(2)
N5-Rh1-Rh2-N7	29.547	22.8(2)
N6-Rh1-Rh2-N8	30.452	22.8(2)

Table S1. continued

3	**Calculated**	**X-ray Data**
	Bond distances (Å)	**Bond distances (Å)**
Rh1-Rh2	2.521	2.5135(9)
Rh1-N4	2.042	2.023(6)
Rh1-N1	2.039	2.024(6)
Rh1-N7	2.049	2.007(8)
Rh1-N8	2.048	2.004(6)
Rh1-N11	2.214	2.225(7)
Rh2-N3	2.042	2.017(6)
Rh2-N6	2.039	2.011(6)
Rh2-N9	2.047	2.024(6)
Rh2-N10	2.048	1.996(7)
Rh2-N12	2.214	2.202(7)
	Dihedral angles (°)	**Dihedral angles** (°)
N3-Rh1-Rh2-N1	23.8	20.2(2)
N6-Rh1-Rh2-N4	23.8	20.6(2)
N7-Rh1-Rh2-N9	34.2	22.7(3)
N8-Rh1-Rh2-N10	34.2	23.0(3)
4	**Calculated**	**X-ray Data**
	Bond distances (Å)	**Bond distances (Å)**
Rh1-Rh2	2.6576	2.655(1)
Rh1-P1	2.2770	2.228(2)
Rh1-C1	2.0289	2.024(5)
Rh1-N1	2.1490	2.131(5)
Rh1-N2	2.1169	2.127(5)
Rh1-N5	2.2083	2.202(6)
Rh2-P2	2.2777	2.232(7)
Rh2-C2	2.0294	2.05(1)
Rh1-N3	2.1169	2.104(6)
Rh1-N4	2.1500	2.142(6)
Rh1-N6	2.2092	2.196(6)
	Dihedral angles (°)	**Dihedral angles** (°)
P1-Rh1-Rh2-C2	-22.704	-23.0(2)
C1-Rh1-Rh2-P2	-22.759	-21.1(5)
N1-Rh1-Rh2-N3	-34.329	-32.3(2)
N2-Rh1-Rh2-N4	-34.386	-31.7(2)

Table S1. continued

5	**Calculated**	**Experimental**
	Bond distances (Å)	**Bond distances (Å)**
Rh1-Rh2	2.6635	2.6262(4)
Rh1-N1	2.1099	2.093(2)
Rh1-N3	2.1107	2.094(2)
Rh2-N2	2.0983	2.078(2)
Rh2-N4	2.0980	2.081(2)
Rh1-C1	1.9420	1.935(2)
Rh1-C2	1.9431	1.948(2)
Rh1-C5	1.9466	1.949(2)
Rh2-C3	1.9463	1.939(2)
Rh2-C4	2.0618	2.080(2)
Rh1-C6	2.0622	2.099(2)
Dihedral angles	**Dihedral angles** (º)	**Dihedral angles** (º)
N1-Rh1-Rh2-N2	19.942	17.79(6)
N3-Rh1-Rh2-N4	20.968	17.97(6)
C1-Rh1-Rh2-C3	29.341	20.48(8)
C2-Rh1-Rh2-C4	30.233	20.99(8)
6	**Calculated**	**X-ray Data**
	Bond distances (Å)	**Bond distances (Å)**
Rh1-Rh2	2.6648	2.6105(9)
Rh1-N1	2.0993	2.097(3)
Rh1-N3	2.1004	2.080(3)
Rh2-N2	2.1125	2.081(3)
Rh2-N4	2.1107	2.094(3)
Rh1-C1	1.9475	1.947(3)
Rh1-C2	1.9469	1.951(4)
Rh1-C5	2.0662	2.074(4)
Rh2-C3	1.9431	1.954(4)
Rh2-C4	1.9442	1.937(4)
Rh1-C6	2.0665	2.134(4)
	Dihedral angles (º)	**Dihedral angles** (º)
N1-Rh1-Rh2-N2	20.624	18.1(1)
N3-Rh1-Rh2-N4	19.600	17.2(1)
C1-Rh1-Rh2-C3	28.747	21.6(2)
C2-Rh1-Rh2-C4	29.716	23.5(2)

Table S1. continued

7	**Calculated**	**X-ray Data**
	Bond distances (Å)	**Bond distances (Å)**
Rh1-Rh2	2.614	2.5860(6)
Rh2-C39	2.066	2.094(5)
Rh2-C31	1.946	1.949(5)
Rh2-C33	1.937	1.946(5)
Rh2-N1	2.113	2.091(4)
Rh2-N4	2.110	2.088(4)
Rh1-N6	2.095	2.077(4)
Rh1-N3	2.105	2.068(4)
Rh1-C37	2.064	2.097(5)
Rh1-C29	1.949	1.939(5)
Rh1-C35	1.951	1.949(5)
	Dihedral angles (°)	**Dihedral angles** (°)
N3-Rh1-Rh2-N1	-20.8	18.9(1)
N6-Rh1-Rh2-N4	-22.5	19.8(1)
C35-Rh1-Rh2-C33	-32.2	21.8(2)
C29-Rh1-Rh2-C31	-32.2	21.0(2)
8	**Calculated**	**X-ray Data**
	Bond distances (Å)	**Bond distances (Å)**
Rh1-Rh2	2.8157	2.7682(6)
Rh1-P1	2.3524	2.2929(9)
Rh1-C1	2.1121	2.090(3)
Rh1-C3	1.9820	2.000(3)
Rh1-C4	2.0053	2.007(2)
Rh1-C7	2.0049	2.023(4)
Rh2-P2	2.3544	2.3077(9)
Rh2-C2	2.1127	2.078(2)
Rh2-C5	2.0047	2.026(3)
Rh2-C6	1.9809	2.009(2)
Rh2-C8	2.0033	2.037(4)
	Dihedral angles (°)	**Dihedral angles** (°)
P1-Rh1-Rh2-C2	-20.302	-21.29(8)
P2-Rh1-Rh2-C1	-20.181	-20.47(8)
C4-Rh1-Rh2-C6	-33.599	-29.4(1)
C3-Rh1-Rh2-C5	-33.512	-35.9(1)

Computational Studies (continued). Density Functional Theory (DFT) calculations were performed using the Gaussian09, Revision B.01 program package.[19] The B3LYP hybrid functional incorporating the Becke three-parameter (B3) exchange functional[20] and the correlation functional of Lee, Yang and Parr (LYP)[21] with the Pople-type basis set 6-311G+(d´)[22] were used for the C, N, H atoms of CH_3CN and CH_3NC, which were calculated in the gas phase. DFT calculations were performed on the cationic units of **1**-**8**. The mPW1PW91 correlation and exchange functionals[23] with the Stuttgart RSC 1997 Electron Core Potential (ECP)[24] basis set were used for the Rh atoms and the 6-31G (d´) basis set[25] for the C, N, F, P and H atoms. The coordinates from the X-ray crystal structures of the cationic units **1**-**3**, **5**-**7** (without the anions) were used as starting points for the geometry optimizations. The *S* isomers from the cationic units of the crystal structures were used for the calculations of **4** and **8**. Frequency calculations were performed on **1**-**8** to confirm that the fully optimized structures were global minima, which is the case for **1**-**6** and **8**. For **7**, however, an imaginary mode was located at -14 cm^{-1}, corresponding to the rotation of one methyl group on the triazenide ligand; this issue, however, did not have a notable effect on the results of the TD-DFT calculations. Based on the gas phase optimized structures for compounds **1**-**8**, a non-equilibrium Time-Dependent Density Functional Theory (TD-DFT)[26] method at the same level, associated with a Polarizable Continuum[27] solvation Model (PCM), was applied in CH_3CN. The first thirty lowest singlet-to-singlet excitations were included in the TD-DFT calculations for the gas phase and the solvation model. For all the compounds, there are slight hypsochromic shifts of the electronic transitions between the gas phase and the solvation model, which are ascribed to the destabilization of the doubly charged compounds in the polarized solvent. The MOs were plotted by using the Agui graphical user interface[28] with an iso-value 0.04 and the detailed analyses for the composition of the orbitals were obtained through the Chemissian program http://www.chemissian.com.

Table S2. Bond Character of Orbitals, Energy Levels (eV) and Orbital Compositions (%) for the Dirhodium Units of **1** and **5**.

	1			**5**		
		Energy (eV)	**Orbital Composition**		**Energy** (eV)	**Orbital Composition**
δ*	HOMO-16	-8.85	43 (DTolF) 42 Rh 15 (eq CH_3CN)	HOMO-16	-9.05	51 Rh 24 (eq CH_3NC) 22 (DTolF)
π	HOMO-15	-8.49	72 Rh 18 (DTolF) 5 (eq CH_3CN)	HOMO-15	-8.88	58 Rh 19 (DTolF) 12 (eq CH_3NC) 11 (ax CH_3NC)
π	HOMO-14	-8.30	80 Rh 9 (eq CH_3CN) 8 (DTolF)	HOMO-14	-8.73	63 Rh 19 (eq CH_3NC) 12 (DTolF) 7 (ax CH_3NC)
δ	HOMO-13	-7.83	79 Rh 13 (DTolF) 8 (eq CH_3CN)	HOMO-13	-8.46	71 Rh 16 (eq CH_3NC) 12 (DTolF)
π*	HOMO-6	-7.28	78 Rh 11 (DTolF) 9 (ax CH_3CN)	HOMO-12	-8.10	81 Rh 9 (eq CH_3NC) 7 (ax CH_3NC)
π*	HOMO-5	-7.25	88 Rh 5 (DTolF)	HOMO-11	-8.08	83 Rh 8 (eq CH_3NC) 6 (ax CH_3NC)
σ	HOMO-4	-7.21	78 Rh 13 (ax CH_3CN)	HOMO-2	-6.76	51 Rh 26 (ax CH_3NC) 14 (DTolF) 9 (eq CH_3NC)
	HOMO[a]	-5.75	71 (DTolF) 27 Rh	HOMO	-5.97	80 (DTolF) 15 Rh
σ*	LUMO	-2.11	66 Rh 12 (DTolF) 16 (ax CH_3CN) 6 (eq CH_3CN)	LUMO	-1.84	63 Rh 13 (DTolF) 14 (ax CH_3NC) 10 (eq CH_3NC)

[a]Not a dirhodium-based orbital.

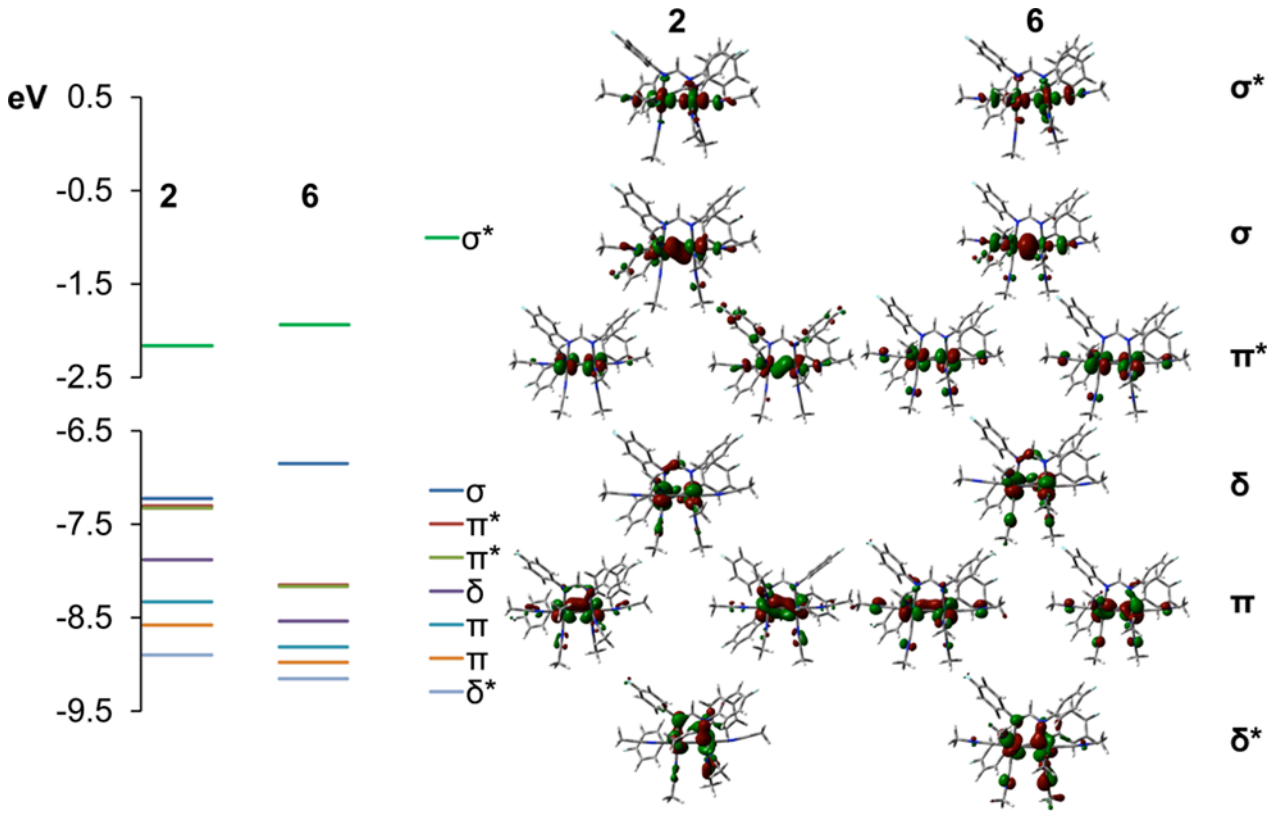

Fig. S9 Diagrams of the MO levels for the dirhodium units in **2** and **6** with visualization of the corresponding orbitals generated by Agui (iso-value=0.04).

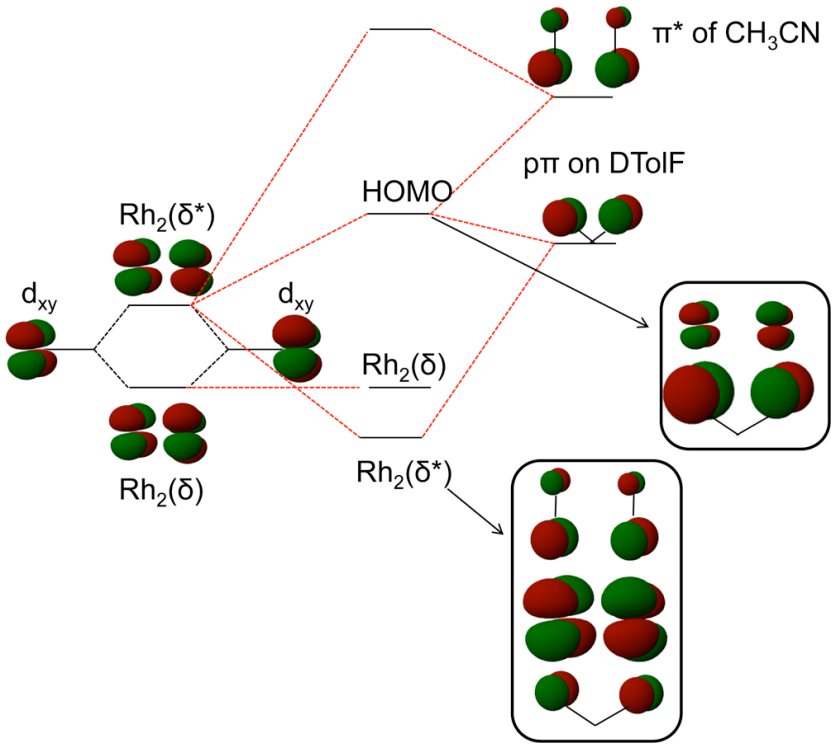

Fig S10. Representation of the orbital interactions between $Rh_2(\delta^*)$, pπ lone pairs on the bridging ligand and the low lying π*orbital on the CH_3NC ligands.

Table S3. Bond Character of Orbitals, Energy Levels (eV) and Orbital Composition (%) for the Dirhodium Units in **3** and **7**.

	3			**7**		
		Energy (eV)	**Orbital Composition**		**Energy** (eV)	**Orbital Composition**
δ*	HOMO-11	-7.68	51 (NNN) 44 Rh	HOMO-18	-9.32	43 Rh 28 (NNN) 25 (eq CH_3NC)
π	HOMO-16	-8.63	74 Rh 12 (NNN) 11 (eq CH_3CN)	HOMO-17	-9.19	63 Rh 14 (NNN) 12 (eq CH_3NC) 11 (ax CH_3NC)
π	HOMO-15	-8.52	49 Rh 42 (NNN) 8 (eq CH_3CN)	HOMO-16	-9.03	63 Rh 20 (eq CH_3NC) 12 (NNN) 5 (ax CH_3NC)
δ	HOMO-13	-8.27	78 Rh 13 (eq CH_3CN) 9 (NNN)	HOMO-15	-8.88	71 Rh 22 (eq CH_3NC) 6 (NNN)
π*	HOMO-10	-7.54	86 Rh 6 (NNN)	HOMO-13	-8.28	64 Rh 21 (NNN) 9 (eq CH_3NC) 6 (ax CH_3NC)
π*	HOMO-9	-7.54	86 Rh 6 (NNN)	HOMO-12	-8.28	53 Rh 32 (NNN) 11 (eq CH_3NC)
σ	HOMO-8	-7.42	45 (NNN) 40 Rh 13 (ax CH_3CN)	HOMO-2	-6.92	46 Rh 24 (ax CH_3NC) 22 (NNN) 7 (eq CH_3NC)
	HOMO	-5.87	79 (NNN) 20 Rh	HOMO	-6.13	86 (NNN) 12 Rh
σ*	LUMO	-2.32	66 Rh 15 (ax CH_3CN) 12 (NNN) 7 (eq CH_3CN)	LUMO	-2.06	65 Rh 16 (NNN) 11 (ax CH_3NC) 9 (eq CH_3NC)

Table S4. Composition (%) of Selected Frontier Molecular Orbitals, Derived from TD-DFT Calculations for **1**-**8**.

	1	**2**	**3**	**4**
HOMO-2	91 (DTolF) 7 Rh	80 (F-form) 17 Rh	92 (NNN) 7 Rh	54 [$Ph_2P(C_6H_4)$] 40 Rh
HOMO-1	93 (DTolF) 5 Rh	90 (F-form) 8 Rh	94 (NNN)	51 [$Ph_2P(C_6H_4)$] 46 Rh
HOMO	71 (DTolF) 27 Rh	69 (F-form) 29 Rh	79 (NNN) 20 (Rh)	68 Rh 20 [$Ph_2P(C_6H_4)$] 10 (ax CH_3CN)
LUMO	66 Rh 16 (ax CH_3CN) 7 (eq CH_3CN)	66 Rh 15 (ax CH_3CN) 12 (F-form) 7 (eq CH_3CN)	66 Rh 15 (ax CH_3CN) 12 (NNN) 7 (eq CH_3CN)	55 Rh 29 [$Ph_2P(C_6H_4)$] 11 (ax CH_3CN) 5 (eq CH_3CN)
LUMO+1	43 Rh 35 (DTolF) 21 (eq CH_3CN)	43 Rh 37 (F-form) 20 (eq CH_3CN)	44 (NNN) 39 (Rh) 16 (eq CH_3CN)	61 [$Ph_2P(C_6H_4)$] 33 Rh 6 (eq CH_3CN)
LUMO+2	45 Rh 33 (DTolF) 22 (eq CH_3CN)	44 Rh 35 (F-form) 21 (eq CH_3CN)	60 (NNN) 36 Rh	63 [$Ph_2P(C_6H_4)$] 29 Rh 7 (eq CH_3CN)

Table S4. Continued

	5	**6**	**7**	**8**
HOMO-2	51 Rh 26 (ax CH_3NC) 14 (DTolF) 9 (eq CH_3NC)	52 Rh 26 (ax CH_3NC) 13 (F-form) 9 (eq CH_3NC)	46 Rh 24 (ax CH_3NC) 22 (NNN) 7 (eq CH_3NC)	76 [$Ph_2P(C_6H_4)$] 21 Rh
HOMO-1	86 (DTolF) 11 Rh	86 (F-form) 10 Rh	90 (NNN) 7 Rh	86 [$Ph_2P(C_6H_4)$] 13 Rh
HOMO	80 (DTolF) 15 Rh	80 (F-form) 15 Rh	86 (NNN) 12 Rh	59 Rh 18 (ax CH_3NC) 15 [$Ph_2P(C_6H_4)$] 9 (eq CH_3NC)
LUMO	63 Rh 14 (ax CH_3NC) 13 (DTolF) 10 (eq CH_3NC)	63 Rh 14 (ax CH_3NC) 14 (F-form) 9 (eq CH_3NC)	65 Rh 16 (NNN) 11 (ax CH_3NC) 9 (eq CH_3NC)	52 Rh 26 [$Ph_2P(C_6H_4)$] 11 (eq CH_3NC) 11 (ax CH_3NC)
LUMO+1	43 Rh 34 (DTolF) 21 (eq CH_3NC)	44 Rh 34 (F-form) 21 (eq CH_3NC)	47 (NNN) 35 Rh 16 (eq CH_3NC)	60 [$Ph_2P(C_6H_4)$] 35 Rh
LUMO+2	41 Rh 36 (DTolF) 19 (eq CH_3NC)	41 Rh 36 (F-form) 19 (eq CH_3NC)	51 (NNN) 38 Rh 8 (eq CH_3NC)	49 [$Ph_2P(C_6H_4)$] 47 Rh

Table S5. Bond Character of Orbitals, Energy Levels (eV) and Orbital Composition (%) for the Dirhodium Units in **8**.

	8		
		Energy (eV)	**Orbital Composition**
π	HOMO-20	-8.59	68 Rh 14 (eq CH_3NC) 12 [$Ph_2P(C_6H_4)$] 6 (ax CH_3NC)
π	HOMO-19	-8.53	67 Rh 13 (eq CH_3NC) 13 [$Ph_2P(C_6H_4)$] 8 (ax CH_3NC)
δ	HOMO-18	-8.38	49 Rh 28 [$Ph_2P(C_6H_4)$] 21 (eq CH_3NC)
δ*	HOMO-17	-8.35	56 Rh 22 [$Ph_2P(C_6H_4)$] 18 (eq CH_3NC)
π*	HOMO-14	-7.89	55 Rh 29 [$Ph_2P(C_6H_4)$] 10 (eq CH_3NC) 6 (ax CH_3NC)
π*	HOMO-13	-7.81	79 Rh 8 [$Ph_2P(C_6H_4)$] 7 (ax CH_3NC) 6 (eq CH_3NC)
σ	HOMO	-6.17	59 Rh 18 (ax CH_3NC) 15 [$Ph_2P(C_6H_4)$] 9 (eq CH_3NC)
σ*	LUMO	-1.67	52 Rh 26 [$Ph_2P(C_6H_4)$] 11 (eq CH_3NC) 11 (ax CH_3NC)

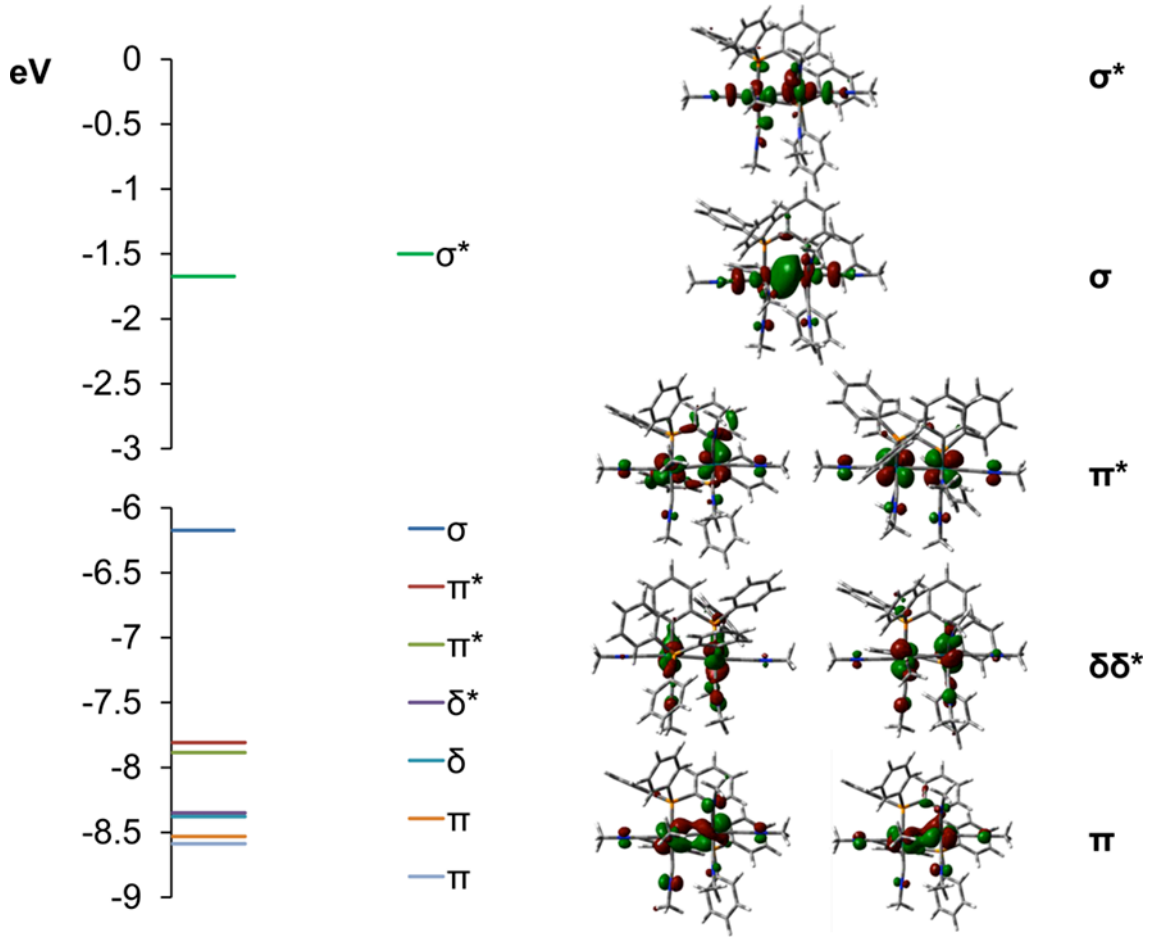

Fig. S11 Diagram of the MO levels for the dirhodium unit in **8** with visualization of the corresponding orbitals generated by Agui (iso-value = 0.04).

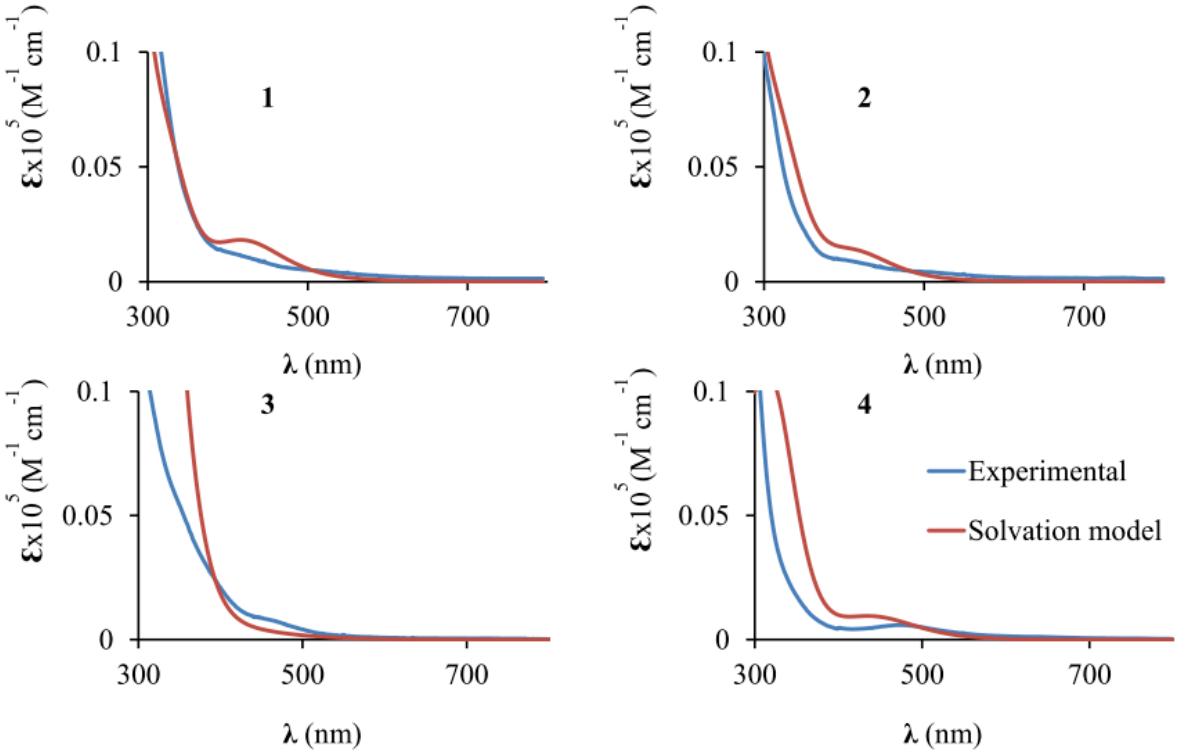

Fig. S12 Overlay of the experimental and calculated electronic absorption spectra (in solvation model with CH_3CN as solvent) for **1-4**.

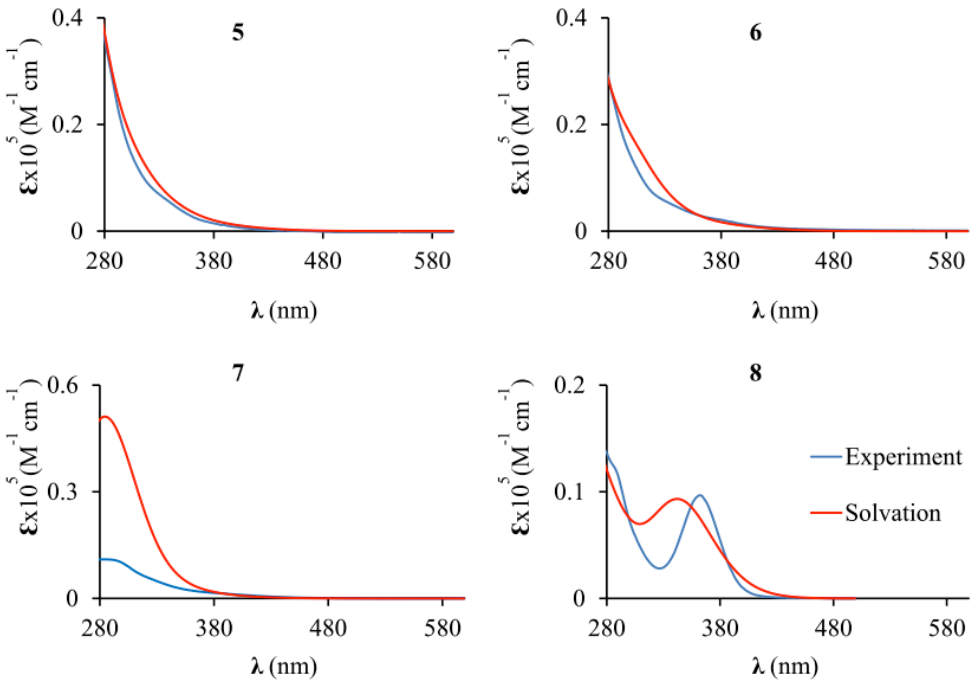

Fig. S13 Comparisons of the experimental and calculated electronic absorption spectra (in solvation model with CH_3CN as solvent) for **5-8**.

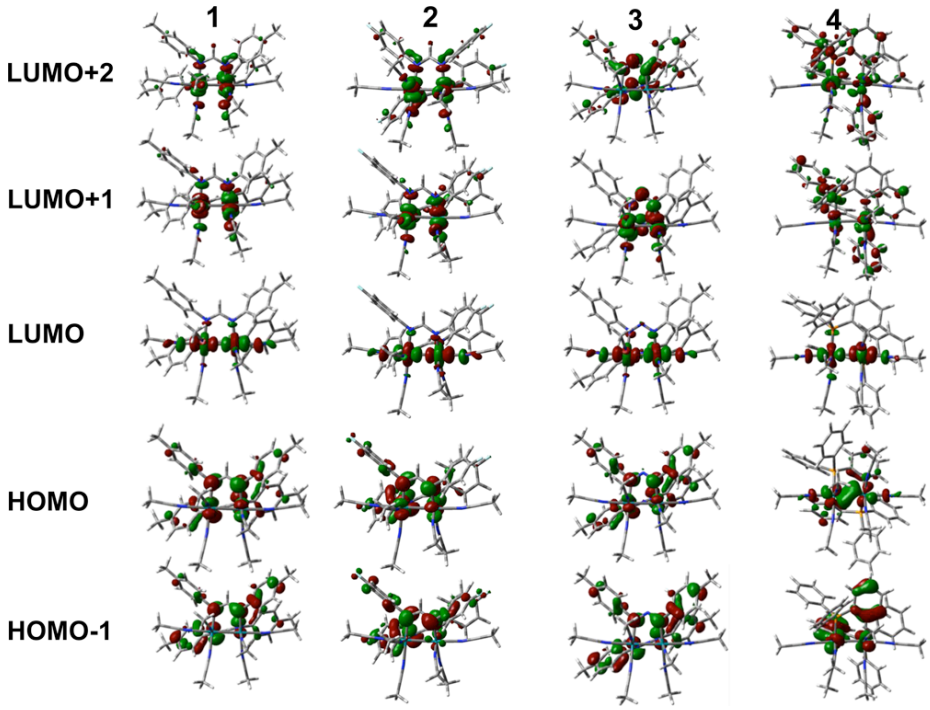

Fig. S14 Visualization of the frontier molecular orbitals mainly involved in the electronic transitions for the DFT calculations of **1**-**4** (iso-value 0.04).

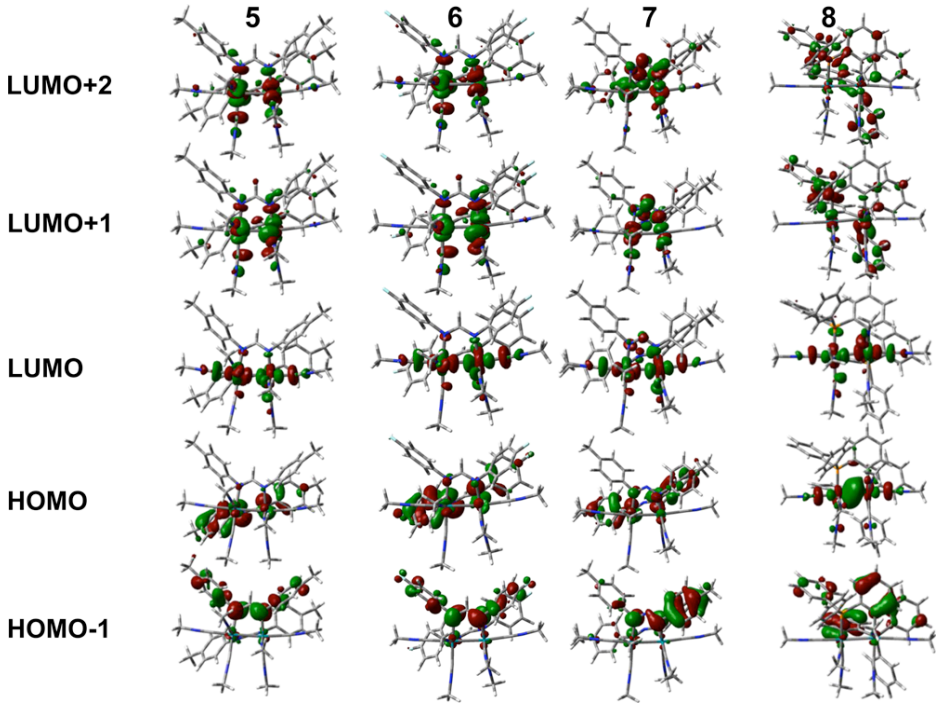

Fig. S15 Visualization of the frontier molecular orbitals mainly involved in the electronic transitions for the DFT calculations of **5**-**8** (iso-value 0.04).

Table S6. Excited states calculated by TD-DFT/PCM (CH_3CN as the solvent) with major transitions* involved in the excitations, transition coefficients, vertical excitation energies (nm), and oscillator strengths (f) for **1** and **2.**

	1				**2**			
state	excitations		E/ nm	f	excitations		E/ nm	f
1	H ->L	94.1%	538	0.0015	H ->L	93.6%	525	0.0011
2	H-6 ->L	30.2%	441	0.0099	H-1 ->L	22.3%	442	0.0019
	H-1 ->L	39.8%						
3	H-5 ->L	88.3%	435	0.0001	H-5 ->L	64.2%	436	0.0001
					H-4 ->L	20.51%		
4	H-6 ->L	22.5%	424	0.0201	H-1 ->L	21.84%	419	0.0150
	H-1 ->L	37.0%			H ->L+1	44.81%		
5	H-1 ->L	20.4%	417	0.0001	H-1 ->L	50.20%	411	0.0066
	H ->L+1	58.9%			H ->L+1	27.31%		
6	H ->L+2	73.6%	405	0.0153	H ->L+2	67.97%	399	0.0097
7	H-1 ->L+1	82.2%	332	0.0001	H-1 ->L+1	58.27%	333	0.0305
8	H-13 ->L	22.8%	330	0.0404	H-15 ->L	17.00%	330	0.0268
	H-2 ->L	27.2%			H-12 ->L	12.88%		
9	H-14 ->L	32.9%	326	0.0010	H-13 ->L	27.34%	326	0.0064
10	H-13 ->L	27.0%	325	0.0044	H-13 ->L	36.90%	323	0.0016

* $2|coefficient|^2 > 0.2$

Table S7. Excited states calculated by TD-DFT/PCM (CH_3CN as the solvent) with major transitions* involved in the excitations, transition coefficients, vertical excitation energies (nm), and oscillator strengths (f) for **5** and **6**.

	5				**6**			
state	excitations		E/ nm	f	excitations		E/ nm	f
1	H-1 ->L	20.17%	413	0.0016	H ->L	77.15%	409	0.0011
	H ->L	75.05%						
2	H-1 ->L	75.81%	392	0.0154	H-1 ->L	78.10%	387	0.0167
	H ->L	20.77%						
3	H ->L+1	74.6%	348	0.0259	H ->L+1	76.39%	345	0.0211
4	H ->L+2	68.89%	337	0.0037	H ->L+2	70.46%	334	0.0044
5	H-1 ->L+1	63.51%	334	0.0501	H-1 ->L+1	64.84%	331	0.0386
6	H-1 ->L+2	68.86%	326	0.0192	H-1 ->L+2	69.27%	324	0.0146
7	H-12 ->L	21.07%	301	0.1654	H-12 ->L	29.91%	301	0.1480
	H-2 ->L	44.98%			H-2 ->L	38.4%		
8	H-11 ->L	43.58%	298	0.0189	H-11 ->L	65.98%	299	0.0234
9	H-2 ->L+1	50.98%	296	0.0403	H-2 ->L+1	46.97%	296	0.0192
10	H-12 ->L	26.65%	295	0.0349	H-12 ->L	25.90%	295	0.1088
	H-3 ->L	24.71%			H-2 ->L	25.93%		

$2|coefficient|^2 > 0.2$

TD-DFT Calculation Analysis for 3 and 7. The lowest energy transition in **3** is of the same character as the transitions in **1** and **2** and it occurs at λ 538 nm (f = 0.0006) (Table S8, ESI). The second set of absorption bands in the region 440-450 nm corresponds to transitions from HOMO, HOMO-1 to LUMO, LUMO+1 orbitals. The excited states 4, 5 centered at λ ~ 425 nm, with low oscillator factors, mainly are $Rh_2(\pi^*) \rightarrow Rh_2(\sigma^*)$ transitions. In the region 340-380 nm, the bands are anticipated to be strong and originate from HOMO, HOMO-1 to the low-lying orbitals including LUMO+1 to LUMO+4 orbitals. Similarly to **5** and **6**, the first two electronic transitions for **7** are mainly HOMO and HOMO-1 to LUMO occurring at λ = 413 and 388 nm (f = 0.0024 and 0.0008, respectively). These hypsochromic shifts, as compared to **3**, are also due to the larger HOMO-LUMO energy gap. The excited states 3-5 arise from HOMO, HOMO-1 to LUMO+1 and LUMO+2 transitions in the region 360-340 nm, and have similar characters and energies to those in **5** and **6**.

Table S8. Excited states calculated by TD-DFT/PCM (CH_3CN as the solvent) with major transitions involved in the excitations, transition coefficients, vertical excitation energies (nm), and oscillator strengths (f) for **3** and **7**.

	3			**7**		
state	excitations	E/ nm	f	excitations	E/ nm	f
1	H ->L 94.15%	538	0.0006	H ->L 91.41%	413	0.0024
2	H ->L+1 62.21%	452	0.0030	H-1 ->L 90.98%	388	0.0008
3	H-1 ->L 56.63%	437	0.0029	H ->L+1 81.08%	361	0.0298
4	H-10 ->L 81.03%	430	0.0003	H-1 ->L+1 72.77%	349	0.0060
5	H-9 ->L 61.44% H-1 ->L 24.54%	424	0.0005	H ->L+2 75.31%	336	0.0028
6	H ->L+4 69.52%	382	0.0107	H-2 ->L 47.27% H-1 ->L+2 30.88%	325	0.0282
7	H-1 ->L+1 88.11%	366	0.0006	H-2 ->L+1 63.75%	318	0.0078
8	H ->L+2 94.51%	347	0.0198	H-1 ->L+2 36.39%	315	0.0853
9	H ->L+3 44.82%	340	0.1346	H ->L+3 52.51%	302	0.2781
10	H-10 ->L+1 48.22%	331	0.0428	H-13 ->L 34.27% H-3 ->L 30.09%	302	0.0175

$2|coefficient|^2 > 0.2$

Table S9. Excited states calculated by TD-DFT/PCM (CH_3CN as the solvent), with major transitions involved in the excitations, transition coefficients, vertical excitation energies (nm), and oscillator strengths (f) for **4** and **8**.

	4			**8**		
state	excitations	E/ nm	f	excitations	E/ nm	f
1	H-4 ->L 24.82% H ->L 48.85%	442	0.0223	H ->L 87.54%	346	0.2222
2	H-3 ->L 67.17% H-1 ->L 22.08%	441	0.0000	H ->L+1 83.60%	312	0.0012
3	H-3 ->L 22.51% H-1 ->L 64.24%	364	0.0012	H ->L+2 67.77%	306	0.0183
4	H-4 ->L 32.91% H-2 ->L 34.18% H ->L 20.00%	359	0.0074	H-2 ->L 72.75%	294	0.0007
5	H-14 ->L 15.07% H-2 ->L 18.65%	327	0.1063	H ->L+2 20.60% H ->L+3 38.38%	290	0.0108
6	H-17 ->L 22.26%	322	0.0027	H-13 ->L 65.68%	288	0.0021
7	H-2 ->L 26.04%	317	0.1262	H-3 ->L 50.27%	287	0.0349
8	H ->L+1 44.44%	312	0.0017	H-1 ->L 43.00% H ->L+3 22.18%	285	0.0959
9	H ->L+2 29.04%	308	0.0009	H ->L+4 79.91%	284	0.0010
10	H-3 ->L+1 32.76%	299	0.0056	H ->L+5 80.72%	269	0.0007

* $2|coefficient|^2 > 0.2$

Table S10. The ν(CN) (cm^{-1}) for the CH_3CN Stretches in the Free Ligand and **1**-**4**.

Compound	ν(CN) (cm^{-1})
CH_3CN	2253
1	2326(w), 2303(m), 2276(w)[a]
2	2334(w), 2308(m), 2276(w)[a]
3	2330(m), 2310(m), 2280(w)[a]
4	2314(m), 2286(sh), 2268(m)[a]
$[Rh_2(CH_3CN)_{10}][BF_4]_4$[b]	2300(w), 2317(m), 2342(m)[c]
$[Rh_2(CH_3CN)_{10}][CF_3SO_3]_4$[b]	2286(m), 2316(w), 2345(m)[c]

[a]Nujol mull, KBr. [b] Ref. [29] [c]Nujol mull, CsI.

References

1 Ugi, U. Fetzer, U. Eholzer, H. Knupfer and K. Offerman *Angew. Chem., Int. Ed.*, 1965, **4**, 472-484.

2 W. W. Hartman and J. B. Dickey, *Org. Synth.*, 1934, **14**, 24.

3 P. Piraino, G. Tresoldi and F. Faraone, *J. Organomet. Chem.,* 1982, **224**, 305-312.

4 N. G. Connelly, H. Daykin and Z. Demidowicz, *J. Chem. Soc., Dalton Trans.,* 1978, 1532-1536.

5 K. V. Catalan, J. S. Hess, M. M. Maloney, D. J. Mindiola, D. L. Ward and K. R. Dunbar, *Inorg. Chem.,* 1999, **38**, 3904-3913.

6 H. T. Chifotides, K. V. Catalan and K. R. Dunbar, *Inorg. Chem.,* 2003, **42**, 8739-8747.

7 A. R. Chakravarty, F. A. Cotton, D. A. Tocher and J. H. Tocher, *Organometallics,* 1985, **4**, 8-13.

8 M. E. Evans and W. D. Jones, *Organometallics,* 2011, **30**, 3371-3377.

9 E. M. Hyde, J. D. Kennedy and B. L. Shaw, *J. Chem. Soc., Dalton Trans.,* 1977, **16**, 1571-1576.

10 SAINT, Program for area detector absorption correction, Siemens Analytical X-Ray Instruments Inc., Madison, WI 53719, USA, 1994-1996.

11 G. M. Sheldrick, SADABS, Program for Siemens area detector absorption correction, University of Göttingen, Göttingen, Germany, 1996.

12 *(a)* L. J. Barbour, X-Seed, Graphical interface to SHELX-97 and POV-Ray, 1999 (http://www.x-seed.net). *(b)* L. J. Barbour, *J. Supramol. Chem.*, 2001, **1**, 189-191. *(c)* J. L. Atwood and L. J. Barbour, *Cryst. Growth Des.*, 2003, **3**, 3-8.

13 G. M. Sheldrick, *Acta Crystallogr. Sect. A,* 2008, **A64**, 112-122.

14 G. Pimblett, C. D. Garner and W. Clegg, *J. Chem. Soc., Dalton Trans.,* 1986, 1257-1263.

15 K. R. Dunbar, S. O. Majors and J. S. Sun, *Inorg. Chim. Acta,* 1995, **229**, 373-382.

16 N. G. Connelly, T. Einig, G. G. Herbosa, P. M. Hopkins, C. Mealli, A. G. Orpen, G. M. Rosair and F. Viguri, *J. Chem. Soc., Dalton Trans.,* 1994, 2025-2039.

17 F. A. Cotton, C. A. Murillo, S. E. Stiriba, X. P. Wang and R. M. Yu, *Inorg. Chem.,* 2005, **44**, 8223-8233.

18 F. A. Cotton, C. A. Murillo, X. P. Wang and R. M. Yu, *Inorg. Chem.,* 2004, **43**, 8394-8403.

19 Gaussian 09, Revision B.01: M. J. Frisch, G. W. Trucks, H. B. Schlegel, G. E. Scuseria, M. A. Robb, J. R. Cheeseman, G. Scalmani, V. Barone, B. Mennucci, G. A. Petersson, H. Nakatsuji,

M. Caricato, X. Li, H. P. Hratchian, A. F. Izmaylov, J. Bloino, G. Zheng, J. L. Sonnenberg, M. Hada, M. Ehara, K. Toyota, R. Fukuda, J. Hasegawa, M. Ishida, T. Nakajima, Y. Honda, O. Kitao, H. Nakai, T. Vreven, J. A. Montgomery, Jr., J. E. Peralta, F. Ogliaro, M. Bearpark, J. J. Heyd, E. Brothers, K. N. Kudin, V. N. Staroverov, R. Kobayashi, J. Normand, K. Raghavachari, A. Rendell, J. C. Burant, S. S. Iyengar, J. Tomasi, M. Cossi, N. Rega, J. M. Millam, M. Klene, J. E. Knox, J. B. Cross, V. Bakken, C. Adamo, J. Jaramillo, R. Gomperts, R. E. Stratmann, O. Yazyev, A. J. Austin, R. Cammi, C. Pomelli, J. W. Ochterski, R. L. Martin, K. Morokuma, V. G. Zakrzewski, G. A. Voth, P. Salvador, J. J. Dannenberg, S. Dapprich, A. D. Daniels, Ö. Farkas, J. B. Foresman, J. V. Ortiz, J. Cioslowski, and D. J. Fox, Gaussian, Inc., Wallingford CT, 2010.

20 A. D. Becke, *J. Chem. Phys.*, 1993, **98**, 5648-5652.

21 C. Lee, W. Yang and R. G. Parr, *Phys. Rev. B*, 1988, **37**, 785-789.

22 *(a)* G. A. Petersson, A. Bennett, T. G. Tensfeldt, M. A. Allaham, W. A. Shirley and J. Mantzaris, *J. Chem. Phys.,* 1988, **89**, 2193-2218. *(b)* G. A. Petersson and M. A. Allaham, *J. Chem. Phys.,* 1991, **94**, 6081-6090.

23 *(a)* C. Adamo and V. Barone, *J. Chem. Phys.,* 1998, **108**, 664-675. *(b)* J. P. Perdew, J. A. Chevary, S. H. Vosko, K. A. Jackson, M. R. Pederson, D. J. Singh and C. Fiolhais, *Phys. Rev. B,* 1992, **46**, 6671-6687. *(c)* J. P. Perdew, K. Burke and Y. Wang, *Phys. Rev. B,* 1996, **54**, 16533-16539.

24 M. Dolg, H. Stoll, H. Preuss and R. M. Pitzer, *J. Phys. Chem.,* 1993, **97**, 5852-5859.

25 *(a)* A. D. McLean and G. S. Chandler, *J. Chem. Phys.,* 1980, **72**, 5639-5648. *(b)* R. Krishnan, J. S. Binkley, R. Seeger and J. A. Pople, *J. Chem. Phys.,* 1980, **72**, 650-654.

26 *(a)* R. Bauernschmitt and R. Ahlrichs, *Chem. Phys. Lett.,* 1996, **256**, 454-464. *(b)* M. E. Casida, C. Jamorski, K. C. Casida and D. R. Salahub, *J. Chem. Phys.,* 1998, **108**, 4439-4449. *(c)* R. E. Stratmann, G. E. Scuseria and M. J. Frisch, *J. Chem. Phys.,* 1998, **109**, 8218. *(d)* C. Van Caillie and R. D. Amos, *Chem. Phys. Lett.,* 1999, **308**, 249-255. *(e)* C. Van Caillie and R. D. Amos, *Chem. Phys. Lett.,* 2000, **317**, 159-164. *(e)* F. Furche and R. Ahlrichs, *J. Chem. Phys.,* 2002, **117**, 7433-7447. *(f)* G. Scalmani, M. J. Frisch, B. Mennucci, J. Tomasi, R. Cammi and V. Barone, *J. Chem. Phys.,* 2006, **124**, 1-15.

27 *(a)* J. Tomasi, B. Mennucci and R. Cammi, *Chem. Rev.,* 2005, **105**, 2999-3093. *(b)* J. Tomasi, Application of Continuum Solvation Models Based on a Quantum Mechanical Hamiltonian In

Structure and Reactivity in Aqueous Solution, *ACS Symp. Ser.*, Eds. J. C. Cramer and D. G. Truhlar, 1994, Vol. **568**, pp 10-23.

28 Agui 9.2.1, R. D. Dennington II, T. A. Keith and J. M. Millam, Semichem, Inc., Shawnee Mission KS, 2008.

29 *(a)* M. E. Prater, L. E. Pence, R. Clerac, G. M. Finniss, C. Campana, P. Auban-Senzier, D. Jerome, E. Canadell and K. R. Dunbar, *J. Am. Chem. Soc.,* 1999, **121**, 8005-8016. *(b)* G. M. Finniss, E. Canadell, C. Campana and K. R. Dunbar, *Angew. Chem., Int. Ed.,* 1996, **35**, 2772-2774.